The role of coronary plaque volumes in major adverse cardiovascular events

Simon Dasselaar

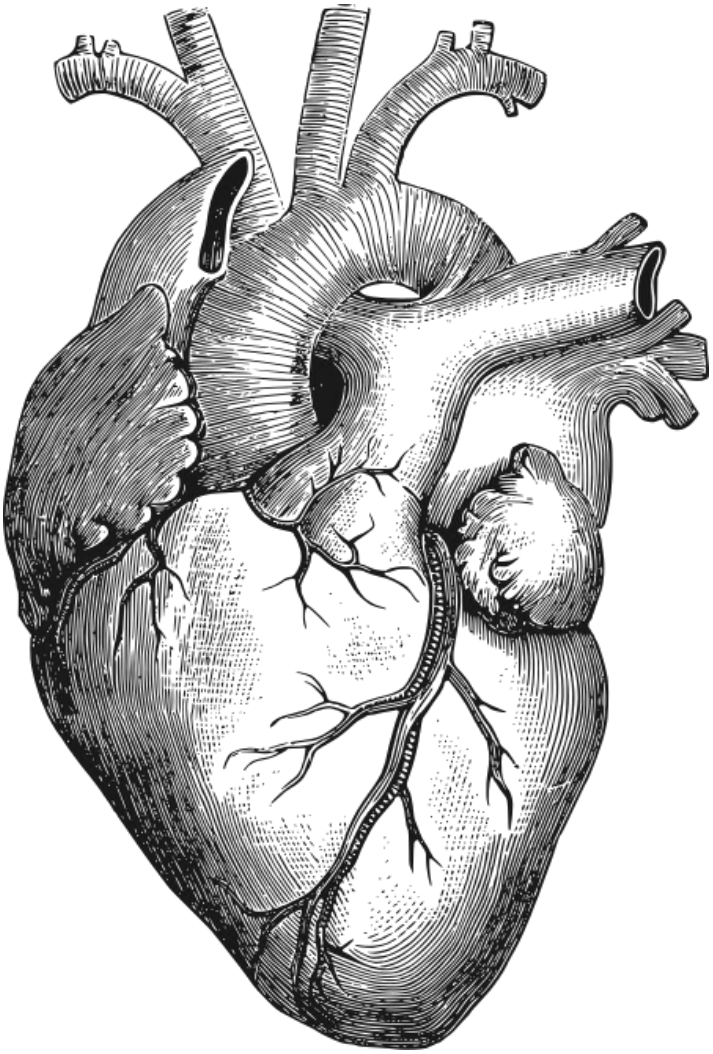

UNIVERSITY
OF TWENTE.

isala

University of Twente

A master's thesis for the degree of Technical Medicine

The role of coronary plaque volumes in major adverse cardiovascular events

Author:
S.G.W. Dasselaar

Graduation committee:
Prof. Dr. J.J. Fütterer
Drs. B.N. Vendel, MD
Dr. C.O. Tan
Dr. J.D. van Dijk, MSc, MBA
Drs. E.M. Walter
Dr. B. Wermelink

07 January 2025

Abstract

Introduction. Coronary computed tomography angiography (CCTA) is a widely used non-invasive imaging technique for assessing coronary artery disease (CAD). It provides detailed images of the coronary arteries, allowing for the detection and characterization of atherosclerotic plaques. This thesis aims to investigate the relationship between different coronary plaque volumes identified through CCTA and the occurrence of major adverse cardiovascular events (MACE) and factors that can affect the plaque volume measurements.

Methods. We retrospectively included all patients who underwent CCTA at Isala hospital between January 2019 and December 2021. Patient data were collected from medical records, and those with incomplete or unassessable scans were excluded. Propensity score matching was used to create comparable groups of patients with and without major adverse cardiovascular events (MACE). Plaque volumes were measured using GE AW-server software. We used Mood's median test and the Mann-Whitney U test to compare the plaque volumes between the no MACE group and MACE group.

Results. A total of 126 patients were included after propensity score matching, 63 with a MACE after CCTA and 63 without a MACE after CCTA with no significant differences in baseline characteristics ($p > 0.05$). Trends in plaque volumes indicated higher overall plaque volumes in the MACE group, with noncalcified and fibro-fatty plaques showing near-significant differences ($p = 0.051$, $p = 0.067$, respectively).

Conclusion. Although we did not find a significant difference in plaque volume between the group that did not experience a MACE after CCTA and the group that did experience a MACE after CCTA, observable trends were present. Non-calcified plaque volumes (< 30 HU) and fibro-fatty plaque volumes (31-130 HU) were generally larger in the MACE group. Additionally, we found that the calcified plaque volumes (>350 HU) were generally smaller in the MACE group compared to the no MACE group.

Acknowledgements

Het afgelopen jaar was een bewogen jaar waarin ik veel heb geleerd, gedaan en meegemaakt. Het ging niet allemaal als gepland maar dankzij goede hulp en motivatie van een groot aantal mensen is het uiteindelijk goed gekomen.

Als eerste wil mijn begeleiders in het Isala bedanken: Brian, Joris en Jorn. Jullie enthousiasme en betrokkenheid hebben mij continu verder geholpen. Jullie waren altijd laagdrempelig bereikbaar en gaven waardevolle feedback die mijn onderzoek steeds verder verbeterde.

Can, bedankt voor je kritische vragen en waardevolle opmerkingen tijdens onze meetings. Jurgen, bedankt dat je bereid was de rol van voorzitter van mijn afstudeercommissie op je te nemen en dat je bereikbaar was voor eventuele vragen over het afstuderen. Bryan, bedankt dat je als buitenlid wilde aansluiten bij mijn afstudeercommissie.

Daarnaast wil ik Elyse bedanken. Je begeleiding en inzichten in mijn persoonlijke ontwikkeling de afgelopen twee jaar waren waardevol. Door jouw goede vragen heb je me aan het denken gezet en hierdoor kon ik mijzelf ook verder ontwikkelen.

Ook wil ik Niels en Marcel bedanken voor het verzorgen van de verschillende fantomen en verder hulp bij het fantoomexperiment.

Mijn speciale dank gaat uit naar de mede-(PhD)studenten: Eline, Jeroen, Levi, Remco en Robin. Bedankt voor de gezellige momenten op kantoor, het wandelen tijdens de lunch, het tafelvoetballen en daarbuiten. Jullie stonden altijd open voor mijn vragen, hoe klein ook, en hebben mijn tijd in het Isala onvergetelijk gemaakt.

Verder wil ik mijn vriendin Maria bedanken. Bedankt dat je er altijd voor mij bent, je enthousiasme en motiverende woorden. Dit gaf telkens weer nieuwe energie.

Tot slot wil ik ook mijn familie bedanken. Jullie onvoorwaardelijke steun en vertrouwen zijn altijd een drijfveer geweest om het beste uit mezelf te halen, niet alleen tijdens mijn studie, maar gedurende mijn hele leven.

Contents

General introduction

Cardiovascular disease (CVD) is the primary cause of mortality globally [1]. Acute coronary syndrome (ACS) frequently serves as the initial clinical presentation of CVD. Coronary artery disease (CAD) is the underlying pathophysiological process that leads to ACS, which is often the first clinical manifestation of CVD[1]. In the Netherlands, CVD was responsible for nearly 23% of all mortality and the second leading cause of mortality, following cancer [2, 3]. CAD is characterized by the progressive development of atherosclerotic plaque in the coronary arteries, leading to increasing stenosis and obstruction which can cause myocardial ischemia [4]. Symptoms associated with CAD are angina which can increase during exertion, dyspnoea, fatigue, or nausea [1, 4, 5].

CAD can be divided into two categories, acute coronary syndrome (ACS), and chronic coronary syndrome (CCS). ACS is diagnosed using rapid assessment tools, including electrocardiograms (ECGs), cardiac biomarkers such as cardiac troponin, and invasive cardiac angiography (ICA) [1]. CCS, on the other hand, is diagnosed through non-invasive imaging techniques like computed tomography-based calcium scoring (CACS), and coronary computed tomography angiography (CCTA) [4]. This research focuses on the quantification of CCTA images.

New CAD-RADS guidelines introduce the possibility of plaque quantification using CCTA images [6]. Research shows that plaque volumes can be used for risk prediction for major adverse cardiovascular events (MACE) [7]. However, these CCTA scans can be made at different tube voltages which can have an effect on the measured CT number and thus on the plaque quantification [8–11]. Furthermore, in literature multiple thresholds are used to determine plaque categories, but there is no standardization yet [11].

The first chapter will give a clinical background of CAD and CCTA. The second chapter will give a technical background in CT, how CT numbers are produced, how iodine contrast gives higher attenuation values, and what the partial volume effect is. Chapter 3 describes a phantom study conducted to assess the influence of tube voltage on CT numbers for different phantom materials. The fourth chapter is a retrospective study performed to find whether plaque quantification can contribute to the risk stratification of patients with CAD.

Clinical Background

Pathophysiology of CAD

Coronary artery disease (CAD) is characterized by the progressive development of atherosclerotic plaques in the coronary arteries[4]. The formation of CAD begins with intimal thickening. This is a response to hemodynamic stress, or the production of sulfate-containing proteoglycans or other forms of extracellular matrix by intimal smooth muscle cells [12]. This causes the first intimal thickening of the intima and lipid accumulation is not yet involved in this process.

Intimal thickening is followed by the development of a fatty streak, marking the initial phase of plaque buildup [13]. This stage is driven by the accumulation of low-density lipoprotein (LDL) cholesterol within the tunica intima layer of the arterial wall. The LDL cholesterol oxidizes in the arterial wall and triggers an inflammatory response, leading to the recruitment of macrophages that ingest LDL particles, which transforms the macrophages into lipid-laden foam cells [14].

Foam cells play a central role in sustaining inflammation [14]. Releasing cytokines and chemokines that recruit additional immune cells including T cells. These T cells further enhance inflammation by producing cytokines which activate the smooth muscle cells in the arterial wall. These smooth muscle cells start to proliferate and migrate towards the inner layers of the artery where they also begin to absorb LDL particles and secrete extracellular matrix components, including collagen, which contribute to plaque growth and structural complexity. These plaques are also called fibro-fatty plaques.

Over time, plaque can either stabilize or continue to grow[14]. If the plaque grows, it can become significant enough to block the blood flow to the myocardial tissue. If there is an increased demand, angina symptoms can occur, which will disappear when the oxygen demand lowers. If the stenosis is ≥90%, it can cause angina at rest. Stable plaques are typically encapsulated by a thick fibrous cap that isolates the necrotic core from the lumen of the artery, reducing the likelihood of a rupture. However, plaques that continue to grow and become unstable, are at a high risk of rupture, which can lead to thrombus (blood clot) formation. Unstable plaques often contain a large necrotic core and a thin fibrous cap, which makes these plaques a high risk of rupture. Plaque rupture is a major cause of thrombosis, often resulting in acute coronary syndromes, such as myocardial infarction. The progression of CAD is also shown Figure 1 [15].

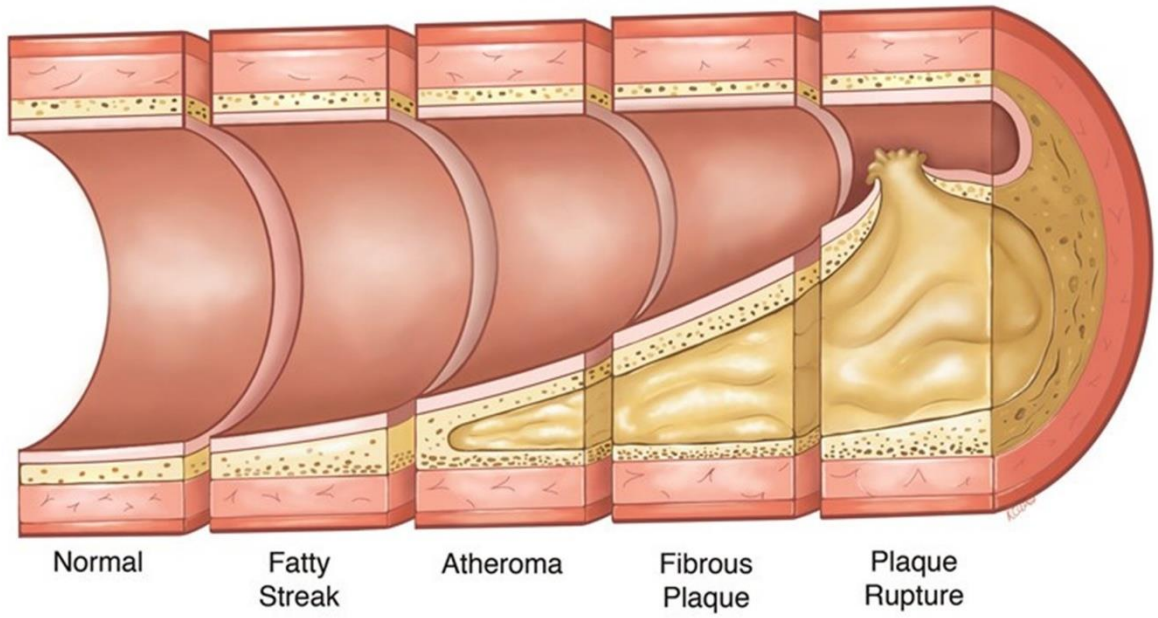

Figure 1: Progression of atherosclerotic plaque [15]

Coronary plaques can also become calcified through several pathways [16]. The first is cell death of the smooth muscle cells. When these cells die, calcium is released and can be deposited in the arterial wall. The macrophages, or foam cells, can release extracellular vesicles, that serve as a framework for the formation of calcium deposits. Genetic factors can also affect the calcification of the coronary plaques. Additional risk factors for coronary calcifications include chronic kidney disease, diabetes, metabolic syndrome, chronic inflammation, aging, postmenopausal women, hyperparathyroidism, and lifestyle factors such as a sedentary lifestyle and a diet high in saturated fats, cholesterol, and refined sugars.

Atherosclerotic plaques, and therefore also coronary plaque can consist of many different components. These different components can be evaluated using coronary computed tomography angiography (CCTA) [7]. Fatty materials exhibit lower attenuation compared to fibrotic components, while calcified components have the highest attenuation.

Fatty materials within the plaques have lower attenuation values, making them appear less dense on the CT images [7]. These fatty deposits are often associated with more vulnerable plaques that are prone to rupture, potentially leading to acute coronary events such as heart attacks. On the other hand, fibrotic components have intermediate attenuation values and represent more stable plaques that are less likely to rupture.

Calcified components, which have the highest attenuation values, indicate the presence of hardened plaques [7]. These calcified plaques are generally more stable but can still contribute to the narrowing of the arteries, reducing blood flow to the heart muscle [17]. The ability to identify and quantify these different components using CCTA provides a comprehensive understanding of plaque composition and helps in evaluating the overall stability of the plaques.

Coronary CT angiography

Coronary CT angiography (CCTA) is the primary diagnostic tool for evaluating coronary anatomy [18]. Heart rate management is important for CCTA scans as higher and irregular heart rates can give motion and step artifacts [19]. Optimal heart rates are typically below 60 beats per minute. Therefore, patients should avoid caffeine as it can elevate their heartrate. Beta-blockers like metoprolol are commonly used to reduce the heartrate of the patients. Before scanning, an iodine based contrast agent is administered through an intravenous line to enhance the contrast of the coronary arteries and helps with identifying plaque buildup and narrowing of the coronary arteries. Segmentation is used to isolate the coronary arteries from the CCTA resulting volume. Post-processing techniques are used to create images that are used for detailed examination of the coronary arteries.

CCTA scans are reported using a standardized system, called Coronary Artery Disease – Reporting and Data System (CAD-RADS). The degree of stenosis is classified using this system and helps to guide patient management [6]. Different degrees of stenosis lead to different CAD-RADS categories. The different CAD-RADS categories, corresponding degree of maximal coronary stenosis and recommendations for further cardiac investigation are shown in Table 1.

Table 1: CAD-RADS reporting and data system for patients with stable chest pain [6]

Category	**Degree of maximal coronary stenosis**	**Further cardiac investigation**
CAD-RADS 0	0% (no plaque or stenosis)	None
CAD-RADS 1	1-24% minimal stenosis or plaque with no stenosis)	None
CAD-RADS 2	25-49% (mild stenosis)	None
CAD-RADS 3	50-69% (moderate stenosis)	Consider functional assessment
CAD-RADS 4a	70-99%	Consider ICA or functional assessment
CAD-RADS 4b	Left main ≥ 50% or 3-vessel obstructive (≥ 70%)	ICA is recommended
CAD-RADS 5	100% (total occlusion)	Consider ICA, functional and/or viability assessment
CAD-RADS N	Non-diagnostic study	Additional/alternative evaluation may be needed

Modifiers can be added to the CAD-RADS score. An example of a modifier is high-risk plaque (HRP) which includes positive remodeling, low-attenuation plaque, spotty calcification and the napkin-ring sign. Plaques with these characteristics have the potential to develop into plaque rupture or thrombosis.

Technical background

CT numbers

Each voxel in a reconstructed CT image is assigned a CT number, also known as a Hounsfield Unit [20]. The CT number is calculated using the following formula:

$$HU = 1000 * \frac{\mu_t - \mu_w}{\mu_w} \text{ [20]}$$

Where μ_t is the linear attenuation coefficient of the tissue in the voxel, and μ_w is the linear attenuation coefficient of water, which serves as a reference. A CT number of 0 HU represents water, air is represented by a CT number of -1000. Every tissue has its own CT number, but by using water as a reference, CT numbers provide a consistent and interpretable representation of tissue density aiding in diagnosis and assessment of various medical conditions.

The photons of an X-ray beam in CT-imaging have a wide range of energies [21]. The energy depends on the tube voltage used during scanning. The higher the tube voltage, the higher the maximum energy of the photons is. Typically, CT scanners operate at tube voltages ranging from 80 to 140 kVp (kilovolt peak), which results in a spectrum of photon energies. This spectrum includes lower energy photons that are more likely to be absorbed by the patient's tissues and higher energy photons that can penetrate more deeply.

Every type of tissue consists of different molecules. Every molecule consists of different atoms and every atom has a specific response to X-rays, determined by its atomic number, electron density, and how it absorbs or scatters X-ray photons [21]. The interaction between X-rays and atoms in a tissue primarily occurs through three mechanisms: photoelectric absorption, Compton scattering and coherent or Rayleigh scattering.

In the process of photoelectric absorption, an X-ray photon interacts with an inner-shell electron of an atom, transferring all its energy to the electron [21]. This interaction results in the ejection of the electron from its shell, creating a photoelectron, and the complete absorption of the incident photon. The probability of photoelectric absorption is highly dependent on the atomic number (Z) of the absorbing material and the energy (E) of the incident photon, which is dependent on the tube voltage [9, 21]. Specifically, the probability is proportional to (Z^3) and inversely proportional to (E^3). This means that materials with higher atomic numbers, such as bone, are more likely to undergo photoelectric absorption, which is why they appear brighter on CT scans.
The ejected electron leaves a vacancy in the inner shell, which is filled by an electron from a higher energy level, resulting in the emission of characteristic X-rays or Auger electrons.

Compton scattering occurs when an X-ray photon collides with an outer-shell electron, the X-ray photon transfers part of its energy to the electron and changes direction [21]. This interaction is more likely to occur in materials with lower atomic numbers, such as soft tissues, where electrons are less tightly bound. The scattered photon retains part of

its original energy. Compton scattering is a significant contributor to background noise in CT images, as it leads to the production of scattered radiation that can degrade image quality. The probability of Compton scattering is relatively independent of the atomic number, but is directly proportional to the electron density of the material.

Coherent or Rayleigh scattering involves the deflection of X-ray photons by atoms without any loss of energy [21]. In this interaction, the incident photon causes all the electrons in the atom to oscillate in phase, and the atom re-emits the photon in a different direction. Since there is no energy transfer, the scattered photon retains its original energy. Coherent scattering is more likely to occur at lower photon energies and in materials with higher atomic numbers. Although this interaction is less significant for image contrast, it can slightly affect image clarity by contributing to the overall scatter radiation.

The combination of these three interactions determines a tissue's attenuation and its corresponding CT number [21]. For example, bone, with a high concentration of calcium, which has a high atomic number, absorbs X-rays more effectively than soft tissues, resulting in higher attenuation and CT numbers. Conversely, air, with a very low atomic density, interacts minimally with X-rays and has lower CT numbers.

Iodine contrast

In CT imaging, many diagnostic tests utilize iodine-based contrast agents. Due to its high atomic number (Z = 53), iodine is highly effective at attenuating X-rays [8]. This strong attenuation is primarily because iodine enhances photoelectric absorption, particularly at the tube voltages used in CT imaging. Since iodine has a K-edge at 33.2 keV, meaning that the electrons in its innermost shell (K-shell) are bound with a binding energy of 33.2 keV. When an X-ray photon has energy just above this value, it can eject a K-shell electron from the atom. This results in high attenuation efficiency for X-ray photons at or near this energy. Consequently, there is a significant increase in contrast between tissues where iodine is concentrated, such as blood vessels or tumors, and the surrounding tissues. Additionally, the high attenuation caused by the iodine contrast can also have an effect on surrounding tissue as it can raise the attenuation of the surrounding tissue as well [22].

Partial volume effect

The partial volume effect is a phenomenon in CT, where a single voxel contains multiple tissue types due to limited spatial resolution [8]. When the boundaries of different tissues fall within the same voxel, the measured signal or attenuation value represents a weighted average of those tissues. This averaging can lead to inaccuracies in image interpretation or measurements, particularly at interfaces between structures of different densities. For example, on the boundary of the lumen of an iodine contrast enhanced artery (300-700 HU) and a soft plaque (-50 – 30 HU) in the wall of the same artery, the voxel can have an averaged CT number that does not accurately represent either material. This effect can impact plaque volume measurements [23].

Variations in Hounsfield Units, a phantom study

Introduction

Computed Tomography (CT) imaging plays a crucial role in medical diagnostics due to its ability to provide detailed cross-sectional images of tissues. CT scans are widely used to diagnose various conditions, including tumors, internal injuries, and cardiovascular diseases [24][25]. One key factor influencing image quality and diagnostic accuracy is the X-ray tube voltage (kV) during scanning[26]. Extensive research has been conducted on kV optimization to enhance image quality and reduce radiation dose [27][28]. Lowering the tube voltage can increase image contrast, especially in iodine-enhanced CT scans, but it also increases image noise [27].

Despite the extensive research on kV optimization, there is limited understanding of how coronary plaque components, such as soft plaque and fibrotic plaque, respond to different tube voltage settings in terms of Hounsfield Units (HU) values [11]. The specific thresholds recommended for distinguishing different types of plaque in the coronary arteries are mostly specified for a single tube voltage [11][29][30]. However, in clinical practice, three types of tube voltages, 120 kV, 100 kV, and 80 kV, are typically used based on patient's body weight, ensuring optimal image quality and minimizing radiation exposure [30]. Different tube voltages can affect the attenuation values of plaque components, potentially leading to variations in diagnostic accuracy [11][31].

In this study, we wanted to investigate how calibrated phantom materials with a specific CT number at 120 kV respond to different tube voltages. By providing quantitative insights into HU variations for different tube voltages, we aim to study whether it is relevant to use different thresholds to determine the composition of coronary plaque for different tube voltages.

Methods

Anthropomorphic chest phantom

A thorax phantom (Thorax-CCI, QRM GmbH, Möhrendorf, Germany) which consists of an anthropomorphic phantom body and a custom water container insert was used for the scans. The anthropomorphic phantom contains artificial lungs and a spine insert surrounded by tissue equivalent material. The outer dimensions of the phantom body are 300*200 mm in transverse plane and 150 mm in height. One extension ring (Extension Ring L, QRM GmbH, Möhrendorf, Germany) was added to the phantom body to enlarge the phantom size in transverse plane to 400*300 mm. The water container was filled with water. In the center of the water container an artery phantom (QRM GmbH, Möhrendorf, Germany) that contains soft plaque components was placed (Figure 2). The artery phantom contains a hollow tube that can be filled with any liquid medium. To the outside of the hollow tube with a diameter of 3 mm, nine calibrated inserts are placed in three sizes (0.5, 1, and 2 mm) around half of the circumference and three calibrated CT numbers at 120 kV (-10, 20, and 50 HU). The entire phantom in the CT-scanner is shown in Figure 3.

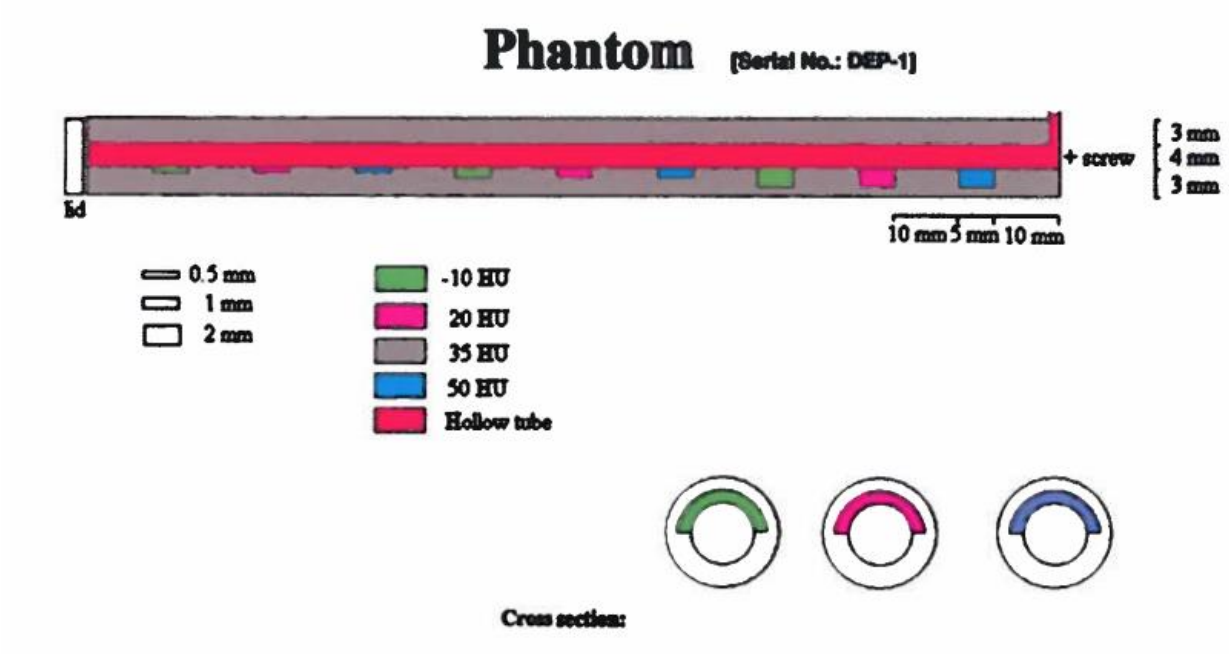

Figure 2: Illustration of the artery phantom (HU: Hounsfield unit).

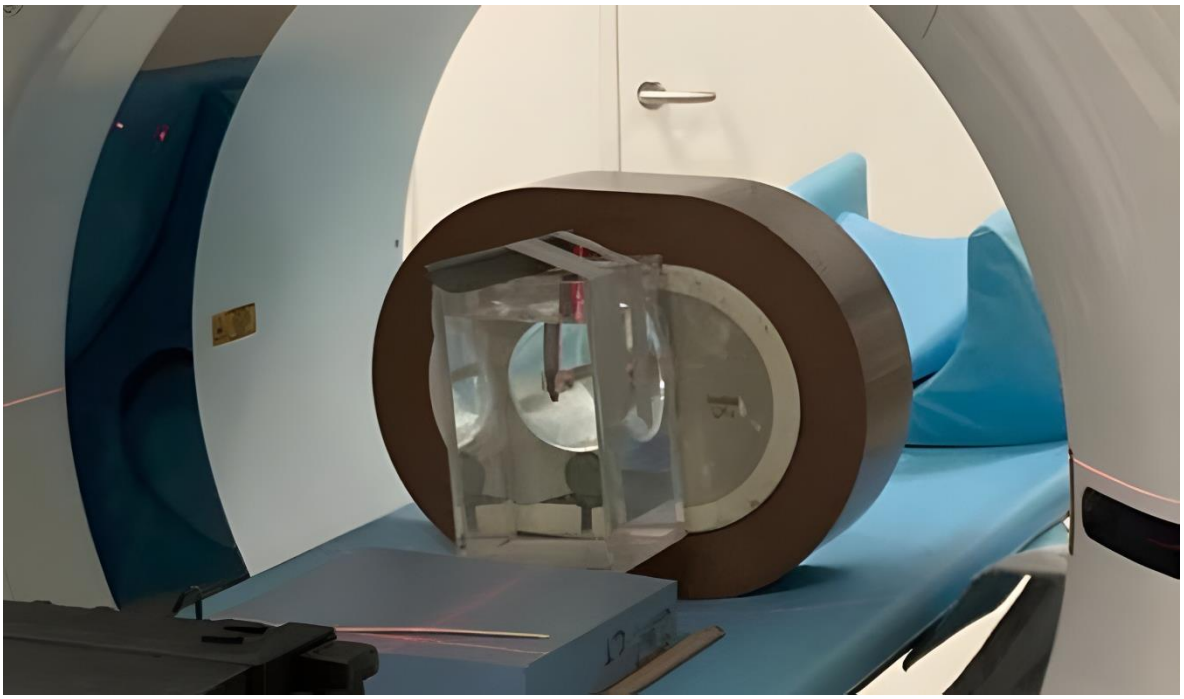

Figure 3: Image of the complete phantom in the CT-scanner

Scan protocol

All CT scans were performed on a 128-rows dual layer detector CT system (Spectral CT 7500, Philips) using a 0.27 seconds of gantry rotation time. A cardiac simulator (Sim4D, QRM GmbH, Möhrendorf, Germany) was used to synthesize ECG signal at a heart rate of 60 bpm. The phantom was placed in the isocenter of the scanner using the laser guides. During the scanning of the phantom, a tube voltage of 120 kV, and a tube current of 991 mA was used to reduce the amount of noise in the images and obtain the most optimal images for analysis. Other scan parameters include slice collimation of 128 x 0.625 mm, and a matrix size of 512 x 512. Because of the dual layer detector, we had the ability to

make different reconstructions for different tube voltages, while scanning using the IDOSE4 reconstruction algorithm.

Analysis
All images of the phantom were analysed using IntelliSpace portal (version 12.1.11, Philips Medical Systems Nederland B.V.), Philips' specific software for image analysis. Using this software, circular regions of interest (ROI) were drawn in different phantom materials. Using the ROIs, a plot was made to evaluate the CT number of different phantom materials for different tube voltages in a 40-200 kV range. Furthermore, the mean CT numbers in Hounsfield Units (HU) and the standard deviation of the different ROI's were measured separately for 80, 100, and 120 kV. We performed measurements on 9 different materials. The measurements were repeated 5 times to increase precision, reduce random error and improve reliability of the measurements.

Statistical analysis
Normality of the data was checked by creating a histogram of each ROI. If the histogram of the ROI shows a bell like curve, normality of the data is assumed. Measurement data was imported into R-Studio (RStudio, Version 2024.9.1.394, Boston, MA, Posit PBC). Repeated measures ANOVA was performed for normally distributed data with tube voltage as the within-subject factor. Effect sizes were calculated using generalized eta-squared (ges). Post-hoc pairwise comparisons using Tukey's Honest Significant Difference (HSD) test were conducted to identify specific differences between tube voltage levels when the ANOVA indicated statistical significance ($p < 0.05$).

Results

The response of the materials to different tube voltages varied. Specifically, the CT number in HU of materials such as artery, fat, spinal cord, lung, perspex, and soft tissue increased for a higher tube voltage. Conversely, the CT number (HU) of the materials air, spine, and water decreased as the tube voltage increased. The standard deviation of all measurements for all materials decreased for higher tube voltages, indicating reduced noise at higher tube voltages. All median and interquartile ranges are shown in Table 2.

Table 2: Median CT number of nine different materials at 80 kV, 100 kV, and 120 kV tube voltages. Each value is accompanied by the interquartile range, reflecting the variability of the measurements for each material across the three tube voltages.

Material	CT number 80 kV (IQR) (HU)	CT number 100 kV (IQR) (HU)	CT number 120 kV (IQR) (HU)
Air	-1000.4 (0.5)	-1000.6 (0.8)	-1000.7 (1.0)
Artery	44.0 (1.8)	50.1 (1.6)	53.2 (1.3)
Fat	-73.1 (1.9)	-64.9 (2.2)	-60.9 (2.4)
Spinal cord	107.5 (0.1)	107.6 (0.2)	107.8 (0.2)
Lung	-803.4 (0.2)	-801.7 (0.4)	-800.9 (0.9)
Perspex	138.6 (4.9)	147.5 (3.3)	151.8 (2.6)
Soft tissue	50.8 (1.2)	60.7 (1.1)	65.0 (1.7)
Spine	343.6 (2.2)	308.4 (1.5)	291.5 (2.7)
Water	-1.1 (1.1)	-1.6 (1.6)	-1.8 (2.0)

Every ROI measurement followed a bell-shaped distribution, and thus, normality was assumed for all measurements. To assess the differences in CT numbers across the different tube voltages (kV) for each material, a repeated measures ANOVA was conducted. Statistical significant differences in CT number were observed across the kV groups for the materials air, artery, fat, lung, perspex, soft tissue, and spine. The effect size for these materials ranged from 0.031 (air) to 0.971 (soft tissue), suggesting small differences in CT number for air, but also very large differences in CT number for soft tissue.
Water demonstrated a p-value of 0.051, which is slightly above the threshold for statistical significance. It's very small effect size of 0.047 suggests that tube voltage has an almost negligible impact on the CT number of water.
For spinal cord, the p-value was 0.408, indicating no statistically significant difference, and the small effect size of 0.143 suggests that the tube voltage has minimal influence on the CT number of this material. The results are shown in Table 3.

Table 3: P-values and effect sizes (ges) for CT number differences across tube voltages for different materials.

Material	p-value	Effect size (ges)
Air	0.018	0.031
Artery	<0.001	0.82
Fat	<0.001	0.93
Spinal cord	0.41	0.14
Lung	<0.001	0.85
Perspex	<0.001	0.65
Soft tissue	<0.001	0.97
Spine	<0.001	0.99
Water	0.051	0.047

Post-hoc pairwise comparisons using Tukey's HSD test were performed on materials that showed significant results in the repeated measures ANOVA. For most materials,

significant differences in CT number were found between all tube voltage comparisons (80 kV vs 100 kV, 80 kV vs 120 kV, and 100 kV vs 120 kV), with p-values less than 0.05. Artery, fat, perspex, soft tissue, and spine showed significant differences across all pairwise comparisons. The lung material also displayed significant differences between 80 kV vs 100 kV and 80 kV vs 120 kV, but the difference between 100 kV and 120 kV was only marginally significant (p = 0.048). However, air shows only a significant difference between 100 kV vs 120 kV. These results indicate that the tube voltage has a measurable effect on the CT number of artery, fat, lung, perspex, soft tissue, and spine materials tested. The results are illustrated in Figure 4, and shown in Table 4.

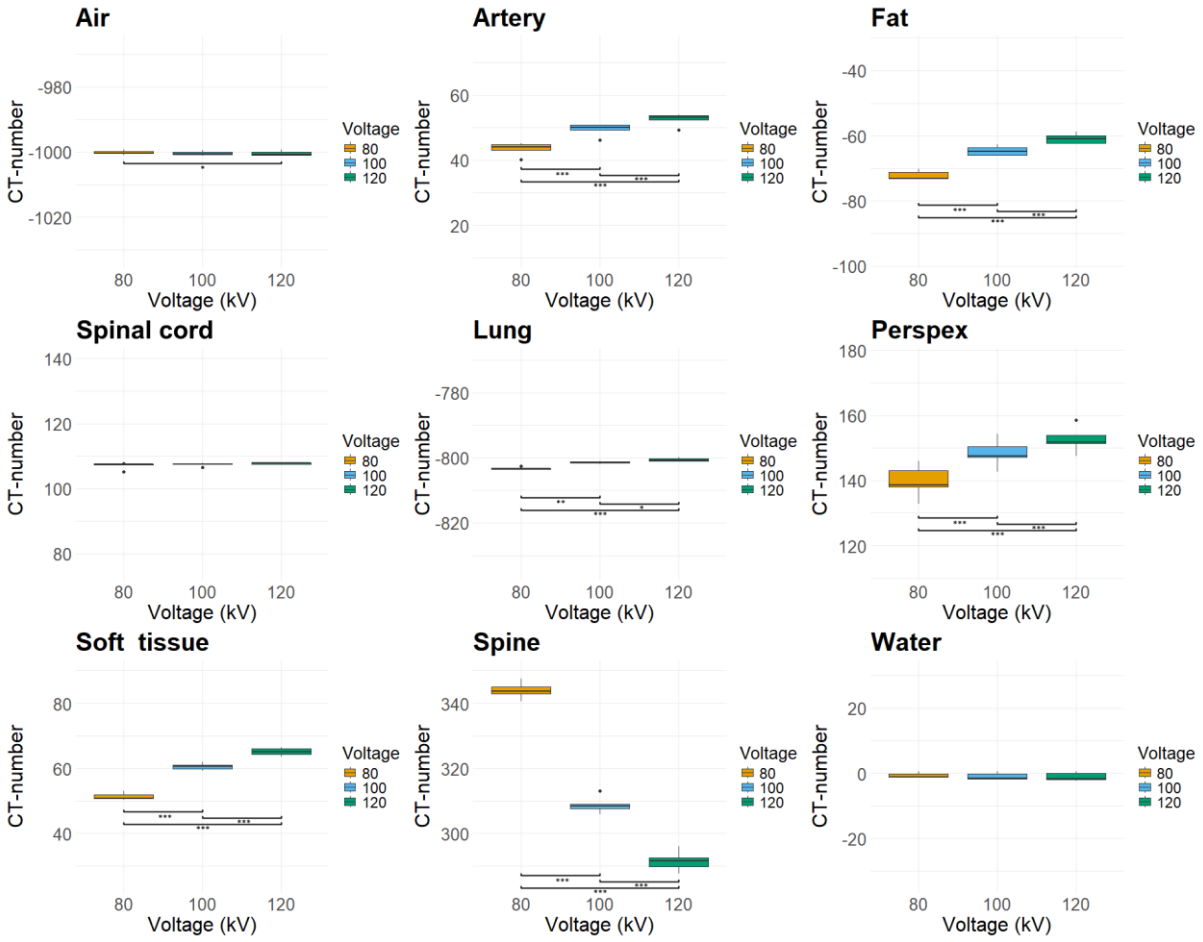

Figure 4: Boxplot showing the CT-number across tube voltages (80, 100, and 120 kV) for different materials. (p < 0.05, ** p < 0.01, *** p<0.001)*

Table 4: Post-hoc Tukey's Honest Significant Difference (HSD) test result for CT number differences between tube voltages (80 kV, 100 kV, and 120 kV) for each material.

Material	80 kV vs 100 kV		80 kV vs 120 kV		100 kV vs 120 kV	
	Δ HU	**p-value**	**Δ HU**	**p-value**	**Δ HU**	**p-value**
Air	-0.2	0.061	-0.2	0.019	0.0	0.70
Artery	6.0	<0.001	9.1	<0.001	3.1	<0.001
Fat	7.6	<0.001	11.3	<0.001	3.7	<0.001
Lung	1.8	0.001	2.6	<0.001	0.8	0.048
Perspex	8.7	<0.001	13.0	<0.001	4.3	<0.001
Soft Tissue	9.3	<0.001	13.8	<0.001	4.5	<0.001
Spine	-35.2	<0.001	-52.5	<0.001	-17.3	<0.001

Discussion

The CT number of nine materials was evaluated at three different tube voltages: 80 kV, 100 kV, and 120 kV. The results revealed that the response of materials to changing tube voltages varied across the materials tested. The variability in CT number, as measured by the standard deviation, decreased with increasing tube voltage, indicating reduced measurement noise at higher voltages. Differences were found between tube voltages for several materials (air, artery, fat, lung, perspex, soft tissue, and spine). HU for water ($p = 0.051$) and spinal cord ($p = 0.408$) did not differ between different tube voltages. Overall, the results indicate that the tube voltage has a measurable effect on the CT number of most materials, with varying levels of significance depending on the material.

We observed that the phantom materials we measured could be grouped into two categories based on their CT number response to tube voltage. In the first group, phantom materials displayed decreased CT-number with increasing tube voltage, while for the second group, the CT-number increased.
Our results are consistent with the fundamental principles of physics, particularly the interactions between X-ray photons and matter. These interactions are governed by well-established physical laws.
Materials with a high atomic number (Z), such as iodine, are more effective at absorbing X-rays due to their larger number of protons [8]. At lower tube voltages, the photo-electric effect dominates for these materials. The probability of photoelectric absorption increases with the cube of the atomic number and inversely with the cube of the photon energy [9]. Additionally, the beam hardening effect is more pronounced for high-Z materials [10]. Consequently, at low tube voltages, high-Z materials exhibit higher CT numbers due to the photoelectric effect. As the tube voltage increases, the contribution of the photoelectric effect decreases, and Compton scattering becomes more significant, resulting in a reduction of the CT number [8].
In contrast, materials with a low atomic number, such as hydrogen or oxygen are less effective at absorbing X-ray photons. For low-Z materials, the photo-electric effect is less prominent [8]. Compton scattering is more significant at higher tube voltages, and beam hardening is less significant for these materials [32]. Therefore, at lower tube voltages, the CT number of low-Z materials is generally lower due to the lower probability of photoelectric absorption. At higher tube voltages, the CT numbers for

these materials tend to increase slightly or remain relatively stable, as Compton scattering, which is less dependent on the atomic number and more on the electron density, becomes the dominant mechanism [33][34][26].

Since water and air are used as reference materials in CT, with water having a CT number of 0 and air a CT number of -1000, CT scanners should be calibrated to ensure accurate CT number measurements. Our results indicated that the CT numbers were close to the expected values. However, we observed a significant difference between 80 kV and 120 kV for air. Rhee et al. found similar results for air, attributing the differences to variations in noise at different tube voltages [9]. Another phantom study also described differences for a variety of materials in CT numbers at different tube voltages, highlighting the importance of accurate calibration and correction schemes [35].

Roa et al. conducted a comprehensive study comparing the image quality of six different CT scanners from four different vendors over a six-year period. Their findings revealed notable differences in CT image quality between different vendors and even variations over time for the same CT system [36]. These variations were observed in multiple image quality parameters, including image noise, uniformity, and spatial resolution. The study highlighted that the Hounsfield Units (HU) for different object densities varied not only between different CT scanner models from different vendors but also over time for a single CT scanner. This indicates that both inter-vendor and intra-vendor differences can significantly impact the consistency and accuracy of CT imaging.

Visually, these differences in CT-number for different tube voltages, can be adjusted for using the window width and the window level setting. However, when it comes to measuring absolute values, such as categorizing different types of plaques, this approach can present challenges.

The artery phantom we used with the specific plaques in the lumen, gave some problems. The plaque inserts, with a specific attenuation of -10 HU, 20 HU, and 35 HU, were undetectable with the Philips Spectral CT 7500. Therefore, the phantom was also scanned using the Siemens Naeotom Alpha, a photon counting CT-scanner with a better spatial resolution to ensure that the plaque inserts were incorporated in the artery. It became clear that the plaque inserts were not incorporated, and therefore we could not measure any of the calibrated inserts.

Limitations

The artery phantom we used, which included specific plaques in the lumen, presented some issues. The plaque inserts, with specific attenuations of -10 HU, 20 HU, and 35 HU, were undetectable using the Philips Spectral CT 7500. To address this, we also scanned the phantom using the Siemens Naeotom Alpha, a photon-counting CT scanner with superior spatial resolution, to ensure that the plaque inserts were correctly incorporated into the artery. Upon further examination, it became evident that the plaque inserts were not integrated in the phantom, which prevented us from measuring any of the calibrated inserts.

Furthermore, we only used one scanner for this study, while patients will also be scanned using different CT scanners. Because Roa et al. proved that the measured CT-

number varied between CT scanners, the experiment should be repeated on different scanners to ensure uniformity between different scanners [36]. For the CCTA scans in our hospital, we use a GE Revolution Apex CT scanner which can produce slightly different CT numbers for the materials we measured in our study. Another limitation of our study is the use of dual-energy reconstructions and not actual scans at 80, 100, and 120 kV, which could result in slightly different results.

Clinical implications

Variations in CT numbers due to different tube voltages can impact the accuracy of diagnostic imaging. Accurate CT numbers are crucial for distinguishing between different types of plaque and identifying abnormalities. Inconsistent CT numbers can lead to misdiagnosis or missed diagnoses, particularly in cases where precise plaque characterization is essential.

Our study found differences in the CT numbers of specific materials at different tube voltages. These variations suggest that the thresholds used for coronary plaque characterization can vary with different tube voltages. This variability underscores the need for more research to define specific thresholds for different tube voltages and CT scanners. Establishing these thresholds is essential to ensure the comparability of coronary plaque characterization results across various imaging systems.

Conclusion

In conclusion, our study demonstrated that the CT-numbers of various materials are influenced by tube voltage. This underscores the importance to consider tube voltage effects in diagnostic imaging, especially when absolute values are used for measurements.

The role of coronary plaque volumes in major adverse cardiovascular events

Introduction

Coronary computed tomography angiography (CCTA) is a widely used non-invasive imaging technique for assessing coronary artery disease (CAD) [37]. It provides detailed images of the coronary arteries, allowing for the detection and characterisation of atherosclerotic plaques [37]. Previous studies have demonstrated the utility of CCTA in diagnosing CAD, predicting adverse cardiovascular events, and guiding clinical decision-making [38]. The use of CCTA has been validated in various populations, and its accuracy and prognostic value are well-established [39]. Additionally, CCTA can identify coronary stenosis severity, distinguish plaque morphology, and characterize alterations in plaque structure in response to treatment [40]. CCTA has also been shown to improve cardiovascular risk stratification and prompt timely initiation of preventive treatments [41].

Despite the established benefits of CCTA, there are still gaps in our understanding of plaque characterization and its correlation with clinical outcomes. For example, while CCTA has shown better long-term prognostic value for major adverse cardiac events (MACE) compared to coronary artery calcium scoring in some studies [40][42], its effectiveness in predicting MACE in real-world clinical settings needs further investigation [40]. More data are needed to explore the role of CCTA in predicting MACE and other cardiovascular outcomes over extended follow-up periods [43]. Studies have also highlighted the need for more research into the prognostic value of CCTA in asymptomatic populations and its role in personalized approaches to prevent atherosclerotic cardiovascular disease [40][43].

With this study, we aim to study the relationship between different coronary plaque categories in CCTA and the occurrence of MACE. We used propensity score matching to minimize bias and confounding, ensuring that our comparisons between the MACE and no MACE group were accurate and meaningful. We explored several different plaque categories found in GE AW server software and in literature to explore the best set of categories to use.

Methods

Population

Patients who underwent CCTA (GE Lightspeed VCT XT, GE Healthcare) (Philips Ingenuity CT, Philips) at Isala Hospital (Zwolle, The Netherlands) between January 2019 and December 2021 were retrospectively included. Patient history, characteristics, and clinical data were collected through a review of medical records using CTcue (version 4.11.1, CTcue), HiX (version 6.2, Chipsoft B.V.), and Sectra IDS7 (version 24.1, Sectra AB). Patients whose data were incomplete or corrupt were excluded. Additionally, those whose CCTA scan were unassessable were excluded. The follow-up period for the patients included was two years. Because of the research's retrospective nature, the

Medical Research Involving Human Subjects Act (WMO) was not applicable. The study was approved by the Lokale Haalbaarheid committee in Isala Hospital (Zwolle, The Netherlands). Subjects did provide informed consent for the use of their data for research purposes.

Data Acquisition and Reconstruction
Patients had to abstain from any drinks and food for 2 hours prior to scanning. In preparation for the CCTA scans, patients heart rate were measured 1 hour to 45 minutes before the CCTA scan. Patients with a rest heart rate between 60 and 69 beats per minute received 50 mg metoprolol and patients with a rest heart rate ≥ 70 received 100 mg metoprolol.

CCTA scans were performed using a 64-slice CT-scanner (Lightspeed VCT XT, GE Healthcare) or (Philips Ingenuity CT, Philips). The coronaries were prospectively scanned using ECG-triggering at 75% of the R-R interval. The kV assist technique was used to automatically select the tube voltage (100kV, or 120kV), and tube current (265 – 800 mAs) based on patient size. Scans were set up to include 12 to 16 cm of detector coverage. Other scan parameters include a rotation time of 0.35 seconds (GE Lightspeed VCT XT, GE Healthcare) or 0.4 seconds (Philips Ingenuity CT, Philips), a slice collimation of 64 x 0.625mm, a matrix size of 512 x 512, and a field of view of 12 to 16 cm.

Propensity score matching
We performed propensity score matching (PSM) to create two similar groups, one group who did not experience MACE and a group who did experience MACE. MACE was defined as those who had an ST-elevation myocardial infarction (STEMI), non-ST-elevation myocardial infarction (NSTEMI), unstable angina pectoris (UAP), or all-cause death and cardiovascular death within two years following the CCTA scan. PSM was performed using the following patient characteristics: age, sex, body mass index (BMI), CAD-RADS score, and several cardiovascular risk factors: smoking status, diabetes mellitus, hypercholesterolemia, hypertension, and a family history of cardiovascular disease. Using these characteristics we tried to minimize possible bias and confounding in this study.

The PSM process was conducted using a genetic algorithm, an optimization technique inspired by natural selection. The algorithm starts with an initial set of weights for the variables used for matching to calculate the propensity scores. Subsequently, it iteratively adjusts these weights to improve the balance of variables between the MACE and non-MACE group. During this process, better solutions are selected and combined to produce new solutions. Once the optimal weights to calculate the propensity scores are determined, the algorithm performs nearest-neighbour matching based on the propensity score of each patient. To verify the quality of the matches, we calculated the maximum caliper width and compared it to the caliper width of 0.2 times the standard deviation of the logit of the propensity score as recommended by Austin [44]. Furthermore, we calculated the standardized mean difference (SMD) to assess the balance before and after matching, with an SMD less than 0.1 indicating a negligible difference between the groups. Using this approach, we ensured a well-balanced

matching that minimized selection bias and allowed for more accurate comparisons between the groups regarding their clinical outcomes.

Measurement protocol

The coronary arteries were segmented and labelled with their corresponding anatomical names using AW-server (version 3.2 Ext. 4.9, GE Healthcare) software in the auto coronary analysis module. In situations where the automatically generated centerline was inaccurate, manual adjustments were made to ensure precision. Figure 5 shows how two measurements are placed next to the segmented artery, from the origo to the minimum diameter of 1.5mm or to when the diameter measurement increases while the image shows that the diameter becomes smaller. The first measurement (PlaqueID 1) is the measurement for the LM, and the second measurement (PlaqueID 2) is the measurement for the LAD. With these measurements, the table as shown in Figure 6 is created. By dragging the thresholds to different values, we can create different thresholds for different plaques. By dragging these measurements next to the artery, the lumen volume is measured too. If no plaque is detected in the measured artery, the volume is shown as 0.0 mm^3.

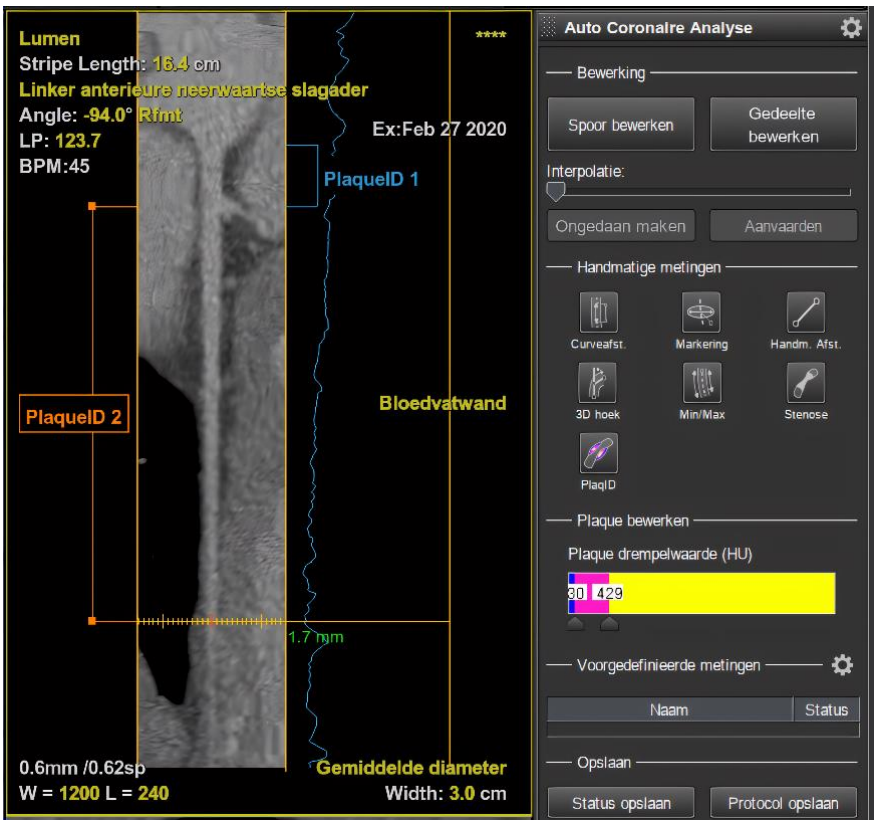

Figure 5: Screencapture of AW server. On the left, the LAD is shown with two measurements: PlaqueID1 and PlaqueID2. PlaqueID1 is the LM, and PlaqueID2 is the LAD. In the image in green is the diameter of the artery shown. On the right, the thresholds are shown in the column with the numbers 30 and 429 which can be dragged to different values to determine plaque volumes for different thresholds.

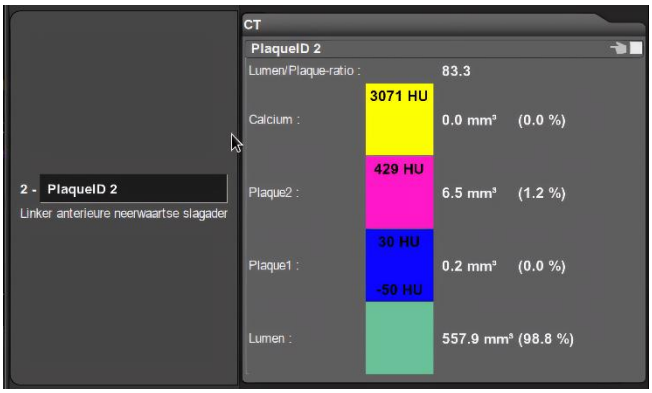

Figure 6: Screencapture of AW server. The table shows the measurement results for the standard thresholds defined by AW server. The screencapture of the AW server shows the measurement results for the standard thresholds of PlaqueID 2. The table includes the lumen volume in mm^3. Plaque1 (non-calcified plaque) is defined as >-50 HU and ≤30 HU, Plaque2 (fibrotic plaque) as >30 HU and ≤429 HU, and Calcium (calcified plaque) as >430 HU, all providing their respective volumes in mm^3.

All arteries with >1.5 mm diameter were measured, following the recommendations provided by GE Healthcare [45]. The AW software automatically determines a threshold to differentiate between fibrotic and calcified plaques. However, the exact method for calculating these thresholds remains undisclosed by GE Healthcare. We investigated the mechanism behind the automatic threshold determination by plotting all thresholds against the attenuation in the aorta for each tube voltage group. To identify the contributing variables, we fitted a linear regression model to these data points. The model included the attenuation in the aorta, the tube voltage, and their interaction as predictors. The adjustable threshold was used as the response variable. Additionally, we performed an ANOVA test to compare two models: one that includes both the attenuation in the aorta and the tube voltage, and another that considers only the attenuation in the aorta.
Next to the automatic threshold determined by the GE AW server software, alternative thresholds, described in literature were also applied to explore which combination of thresholds provides the most accurate assessment. In total, seven plaque volumes, and one lumen volume were measured, and the total plaque-to-lumen ratio was calculated for each artery. All of the measurements and their respective thresholds are described in Table 5.

Table 5: Measurement names, and their corresponding Hounsfield Unit Thresholds and unit

Measurement name	**Hounsfield Unit thresholds**	**Unit**
Noncalcified	-50 – 30 HU	mm^3 or µL
Fibrotic	31 – threshold	mm^3 or µL
Calcified	> threshold	mm^3 or µL
Fibro-fatty	31 – 130 HU	mm^3 or µL
Fibrous	130 – 350 HU	mm^3 or µL
Fibrotic	31 – 350 HU	mm^3 or µL
Calcified	> 350 HU	mm^3 or µL
Lumen		mm^3 or µL
Plaque/lumen		

We performed a maximum of 99 measurements per patient based on 9 measurements per coronary artery. Arteries that were measured are the left main coronary artery, left anterior descending artery, a maximum of two diagonals that split off from the left anterior descending artery, the left circumflex artery, the marginal obtuse artery, the right coronary artery, posterior descending artery, posterior lateral artery, the total of all of the measurements mentioned before, and the largest plaque in the coronary arteries. For analysis, the measurements were summed per perfusion artery. This resulted in the LM perfusion area, LAD perfusion area, LCX perfusion area, and RCA perfusion area, each containing nine measurements.

Statistical analysis

Statistical analysis was performed using RStudio (RStudio, Version 2024.9.0.375, Boston, MA, Posit PBC). To assess the relationship between aortic attenuation and the automatic threshold, we employed linear regression analysis. Separate regression models were fitted to the data from 100 kV and 120 kV scans. To evaluate the impact of kV on the relationship between aortic attenuation and the automatic threshold, a comprehensive linear regression model was constructed. This model included aortic attenuation, kV, and their interaction term as predictors for the adjustable threshold. The significance of each predictor was assessed using t-tests. To determine whether adding kV as a predictor significantly improved the model's fit, an ANOVA comparison was conducted between two nested models. The first model included only aortic attenuation, while the second model incorporated both aortic attenuation and kV.

To assess the impact of kV on plaque characteristics and MACE risk, we conducted a series of univariate analyses. First, we compared plaque measurements between the 100 kV and 120 kV groups for each plaque category. We developed univariate logistic regression models to evaluate the association between individual plaque measurements and MACE, adjusting for kV. Due to the multicollinearity among the plaque measurements, a multivariate analysis was not feasible.

We used Mood’s median test and the Mann-Whitney U test to compare the plaque volumes of the coronary artery with the largest plaque between the no MACE group and the MACE group. Mood’s median test was applied to assess differences in the medians of the plaque categories [46]. The Mann-Whitney U test, a non-parametric test, was used to compare the distribution of the plaque volumes of the different plaque categories between the no MACE and MACE group, providing a measure of whether the ranks of the plaque volumes differ significantly [47].

Results

Study population

We retrospectively included 4,253 patients who underwent CCTA at Isala Hospital between January 1. 2019 and December 31. 2021. Of these, 50 patients were excluded due to unusable CCTA scans for diagnostic purposes (CAD-RADS N). Additionally, 2,503 patients were excluded because of incomplete data, such as missing risk factors. The remaining patients were divided into two groups for propensity score matching: one group comprised patients who did not experience a MACE after CCTA, and the other group included patients who did experience a MACE following CCTA. The inclusion and exclusion process is illustrated in Figure 7. Baseline characteristics of both groups did differ significantly for CAD-RADS categories, other characteristics did not differ significantly as shown in Table 6.

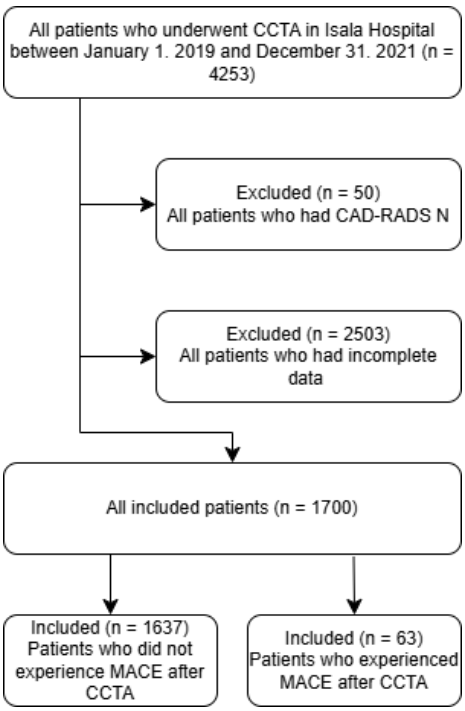

Figure 7: Inclusion flowchart. 50 patients were excluded because of a nondiagnostic CCTA. 2503 patients were excluded because of missing data

Table 6: Baseline characteristics of all 1700 patients who were included before propensity-based matching who either had a MACE or no MACE after CCTA. BMI, body mass index; values are presented as mean ± sd or percentages.

Characteristic		**No MACE (n = 1637)**	**MACE (n = 63)**	**p-value**
Male		803 (49.1%)	37 (58.7%)	0.168
Age (years)		60.13 ± 11.26	60.65 ± 12.05	0.720
Length (cm)		174.84 (9.89%)	174.55 (9.53%)	0.820
Weight (kg)		84.52 ± 16.93	81.66 ± 14.10	0.187
BMI ($kg \cdot m^2$)		27.59 ± 4.75	26.84 ± 4.70	0.222
CAD-RADS	0	452 (27.6%)	6 (9.5%)	<0.001
	1	691 (42.2%)	6 (9.5%)	
	2	342 (20.9%)	10 (15.9%)	
	3	109 (6.7%)	17 (27.0%)	
	4a	38 (2.3%)	20 (31.7%)	
	4b	2 (0.1%)	3 (4.8%)	
	5	3 (0.2%)	1 (1.6%)	
Smoking	Never	473 (28.9%)	31 (42.2%)	0.399
	Ever	931 (56.9%)	23 (36.5%)	
	Present	233 (14.2%)	9 (14.3%)	
Diabetes		122 (7.5%)	9 (14.3%)	0.079
Hypercholesterolemia		638 (39.0%)	31 (49.2%)	0.134
Hypertension		780 (47.6%)	37 (58.7%)	0.110
Family history of CAD		941(57.5%)	39 (61.9%)	0.571

Propensity score matching

After propensity score matching, baseline characteristics of both groups did not differ significantly as shown in Table 7 ($p > 0.05$). In summary, before matching, there was an unbalance for the characteristics propensity distance, age, gender, BMI, CAD-RADS categories 0, 1, 3, and 4a, hypercholesterolemia, and hypertension. This means that the groups being compared (those with and without MACE) were not equivalent in terms of these key characteristics. This lack of balance can introduce bias and confounding factors, potentially skewing the results and leading to inaccurate conclusions about the relationship between CCTA findings and clinical outcomes. The covariates CAD-RADS 2, CAD-RADS 4b, CAD-RADS 5, smoking, diabetes mellitus, and family history of CAD were all already balanced. After matching, the balance of all covariates improved, no imbalance was observed, and the SMD of all covariates was < 0.1, which indicates a good balance, as shown in Figure 8. This indicates that the group with MACE and the group without MACE are equivalent in terms of the characteristics used for matching.

Table 7: Baseline characteristics of all 126 patients who were included after propensity-based matching who either had a MACE or no MACE after CCTA. BMI, body mass index; values are presented as mean ± sd or percentages.

Characteristic		**No MACE (n = 63)**	**MACE (n = 63)**	**p-value**
Male		39 (61.9%)	37 (58.7%)	0.856
Age (years)		61.51 ± 10.72	60.65 ± 12.05	0.674
Length (cm)		175.20 ± 10.12	174.55 ± 9.53	0.709
Weight (kg)		82.93 ± 13.80	81.66 ± 14.10	0.609
BMI ($kg \cdot m^2$)		26.97 ± 3.68	26.84 ± 4.70	0.866
CAD-RADS	0	6 (9.5%)	6 (9.5%)	>0.999
	1	6 (9.5%)	6 (9.5%)	
	2	11 (17.5%)	10 (15.9%)	
	3	17 (27.0%)	17 (27.0%)	
	4a	20 (31.7%)	20 (31.7%)	
	4b	2 (3.2%)	3 (4.8%)	
	5	1 (1.6%)	1 (1.6%)	
Smoking	Never	31 (42.2%)	31 (42.2%)	>0.999
	Ever	23 (36.5%)	23 (36.5%)	
	Present	9 (14.3%)	9 (14.3%)	
Diabetes Mellitus		8 (12.7%)	9 (14.3%)	>0.999
Hypercholesterolemia		31 (49.2%)	31 (49.2%)	>0.999
Hypertension		38 (60.3%)	37 (58.7%)	>0.999
Family history of CAD		40 (63.5%)	39 (61.9%)	>0.999

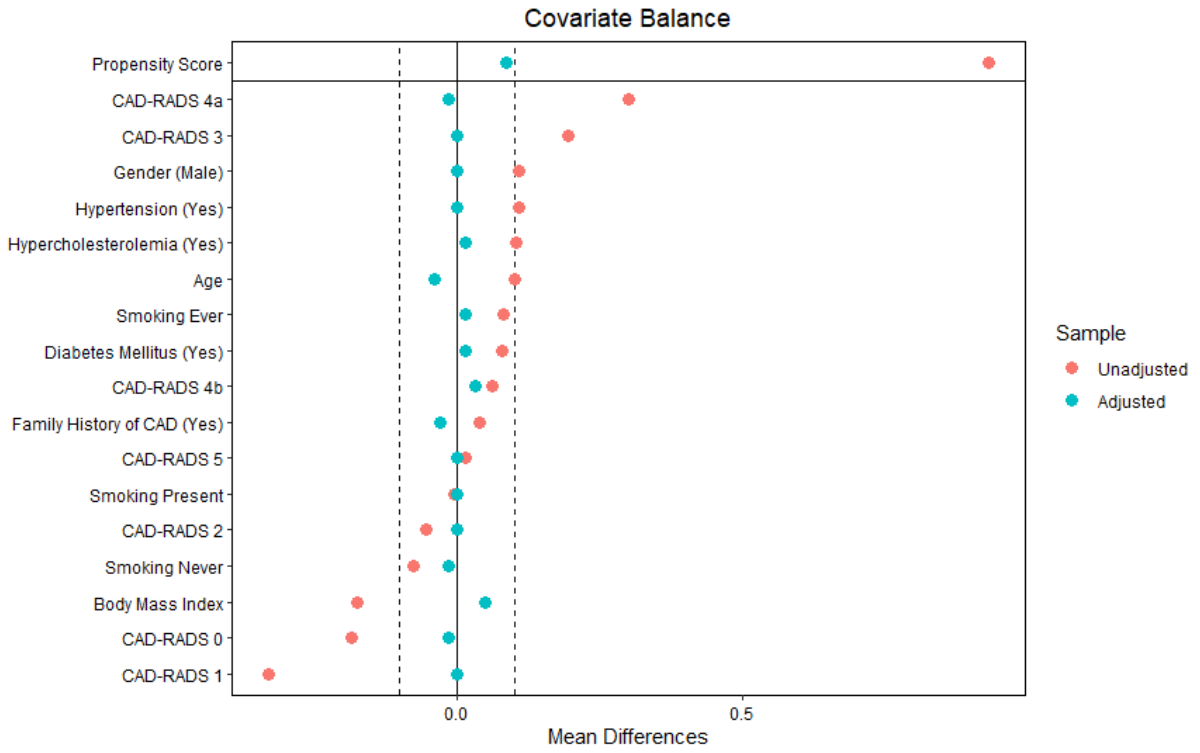

Figure 8: Standardized Mean Differences before and after matching. This figure shows the standardized mean differences (SMDs) for each covariate before and after propensity score matching. The SMDs before matching are represented by blue dots, and the SMDs after matching are represented by red dots. The vertical dashed line at an SMD of 0.1 indicates the threshold below which covariates are considered to be balanced. The plot demonstrates that the matching procedure has substantially improved the balance of covariates between the treated and control groups.

The maximum caliper after matching was 0.1448, while the maximum calculated caliper of 0.2 times the standard deviation of the logit of the propensity score was 0.3203. This indicates a good quality of matches, suggesting that the propensity score matching process effectively balanced the covariates between the groups.

Automatic threshold

To assess how the adjustable threshold works, we plotted the adjustable threshold on the y-axis and the attenuation in the aorta on the x-axis. The R^2 value of the 100 kV model was 0.73, indicating a good fit as the model explains 73% of the variance in the adjustable threshold at 100 kV. In contrast, the R^2 value of the 120 kV model was 0.453, indicating a weaker fit as it explains only 45.3% of the variance. This comparison suggests that the 100 kV model provides a better fit for predicting the adjustable threshold based on the attenuation in the aorta. The model fitted to all data points had an R^2 value of 0.662, explaining 66.2% of the variance, which lies between the values for the 100 kV and 120 kV models. The results are illustrated in Figure 9.

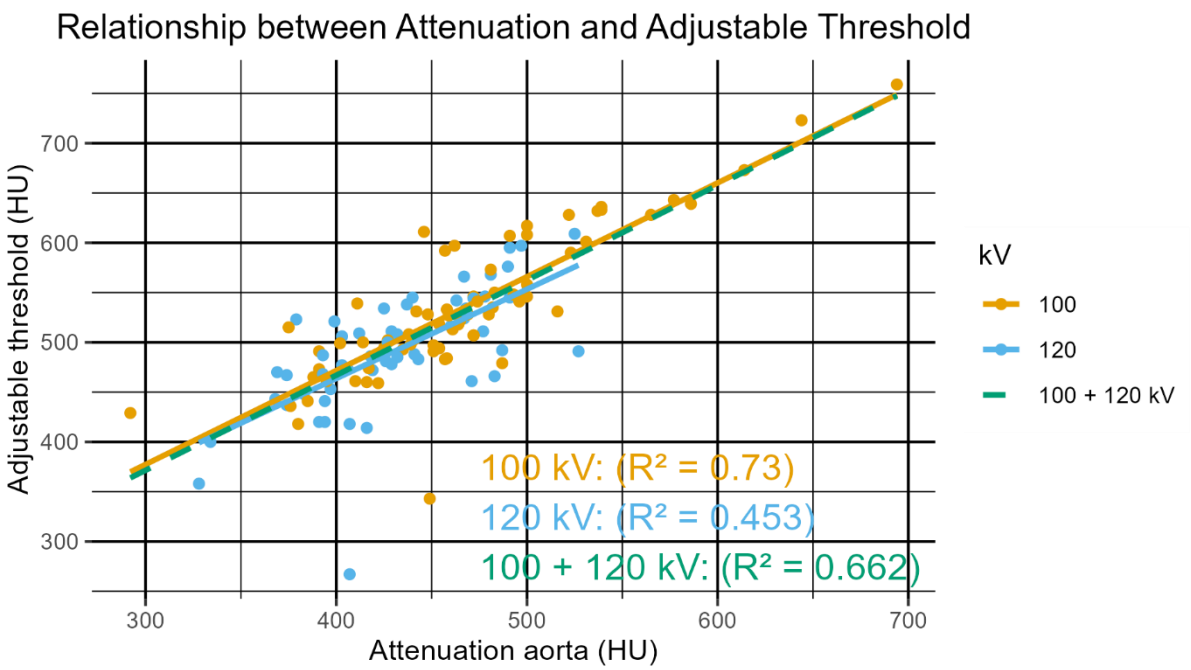

Figure 9: Scatter plot with linear regression lines illustrating the relationship between the attenuation in the aorta and the adjustable threshold. The datapoints are grouped by kV level with separate regression lines for 100 kV and 120 kV in the same color. In green the regression line for the combined data is shown.

A linear regression analysis was conducted to evaluate the impact of the attenuation in the aorta (Attenuation_aorta) and tube voltage (kV 120) on the adjustable threshold. The intercept of the model was estimated to at 94.550 (Std. Error = 35.342, p = 0.008), indicating that when both the attenuation in the aorta and the tube voltage is 120 kV, the adjustable threshold is expected to be 94.550. The coefficient for the attenuation in the aorta was 0.942 (Std. Error = 0.075, p < 0.001), suggesting a significant positive association between the attenuation in the aorta and the adjustable threshold while kV is kept constant. The coefficient for kV120 was 10.445 (Std. Error = 64.195, p = 0.871), indicating that the effect of kV on the adjustable threshold was not statistically significant on the adjustable threshold when the attenuation in the aorta is accounted for. The interaction term Attenuation aorta:kV had a coefficient of -0.046 (std. error = 0.144, p = 0.751), indicating that the interaction between the attenuation in the aorta and kV was also not statistically significant. This implies that the relationship between the attenuation in the aorta and the adjustable threshold does not significantly differ for both levels of kV.

Overall, the results highlight that the attenuation in the aorta is a significant predictor of the adjustable threshold, while kV and its interaction with attenuation in the aorta do not have significant effects, as shown in Table 8.

Table 8: Summary of linear regression model coefficients for the relationship between the attenuation in the aorta and the adjustable threshold. The table presents the estimates (Estimate), standard errors (Std. Error), t-values (T value) and p-values(Pr(>|t|) for the intercept, attenuation in the aorta, 120 kV, and the interaction term attenuation aorta:kV120. Significant p values are highlighted in bold.

Coëfficients	Estimate	Std. Error	T value	Pr(>|t|)
Intercept	94.55	35.34	2.675	**0.008**
Attenuation aorta	0.942	0.075	12.566	**<0.001**
kV 120	10.45	64.20	0.163	0.871
Attenuation aorta:kV 120	-0.046	0.14	-0.318	0.751

The ANOVA comparison between the two linear regression models, one without kV and one with kV, shows that there is no significant difference between the two models (p = 0.202). This means that including the tube voltage (kV) as a predictor does not significantly improve the model's fit compared to the model that only includes the attenuation in the aorta. The full ANOVA results are shown in Table 9.

Table 9: ANOVA comparison of two linear regression models, one that does not consider kV when predicting the adjustable threshold, and one that does consider kV next to the attenuation in the aorta to predict the adjustable threshold. The table shows the residual degrees of freedom (Res. Df.), residual sum of squares (RSS), R^2, degrees of freedom (Df), sum of squares (Sum of Sq.), F-statistic, and p-value (Pr(>F) for the models.

	Res. Df.	RSS	R^2	Df	Sum of Sq	F	Pr(>F)
Model without kV	123	204799	0.667				
Model with kV	124	207540	0.662	-1	-2740.2	1.6457	0.202

Impact of tube voltage on plaque volumes

None of the plaque categories showed a statistically significant association with kV, as all p-values were above the threshold of p = 0.05. The closest plaque category to significance was fibro-fatty plaque (31-130 HU) with a p-value of 0.088. This suggests that while there may be trends, the differences in plaque volumes for the different plaque categories were not statistically significant between 100 and 120 kV. All p-values are shown in Table 10. Because the impact of kV is not significant, we will not correct for differences.

Table 10: Univariate analysis of plaque measurements and MACE adjusted for kV. P-value of kV is shown to focus on the impact of kV on the different plaque categories.

Plaque categories	**P-value kV**
Affected vessel Noncalcified plaque (<30 HU)	0.164
Affected vessel Fibrotic plaque (31-threshold HU)	0.132
Affected vessel calcified plaque (>threshold HU)	0.389
Affected vessel Fibro-fatty plaque (31-130 HU)	0.088
Affected vessel fibrous plaque (131-350 HU)	0.230
Affected vessel fibrotic plaque (31-350 HU)	0.113
Affected vessel calcified plaque (>350 HU)	0.358
Affected vessel lumen volume	0.236
Affected vessel plaque/lumen	0.372

Plaque volumes

The boxplots provide a clear visualization of the distribution of plaque volumes across different categories for the MACE and No MACE groups. In general, the MACE group exhibits higher plaque volumes across all plaque categories, indicating a greater overall burden of plaque in individuals with MACE. This trend is consistent across noncalcified, fibrotic, fibro-fatty, fibrous plaque categories, and the plaque/lumen ratio.

However, an interesting exception is observed in the calcified plaque categories. Both calcified plaque categories (Calcified (>threshold) and Calcified (>350 HU) show smaller volumes in the MACE group compared to the No MACE group. This suggests that while the MACE group has a higher overall plaque burden, the volume of calcified plaques is relatively lower in these individuals. This finding could imply differences in the composition and stability of plaques between the two groups, potentially influencing the risk and outcomes associated with MACE. All plaque categories are illustrated using boxplots in Figure 10.

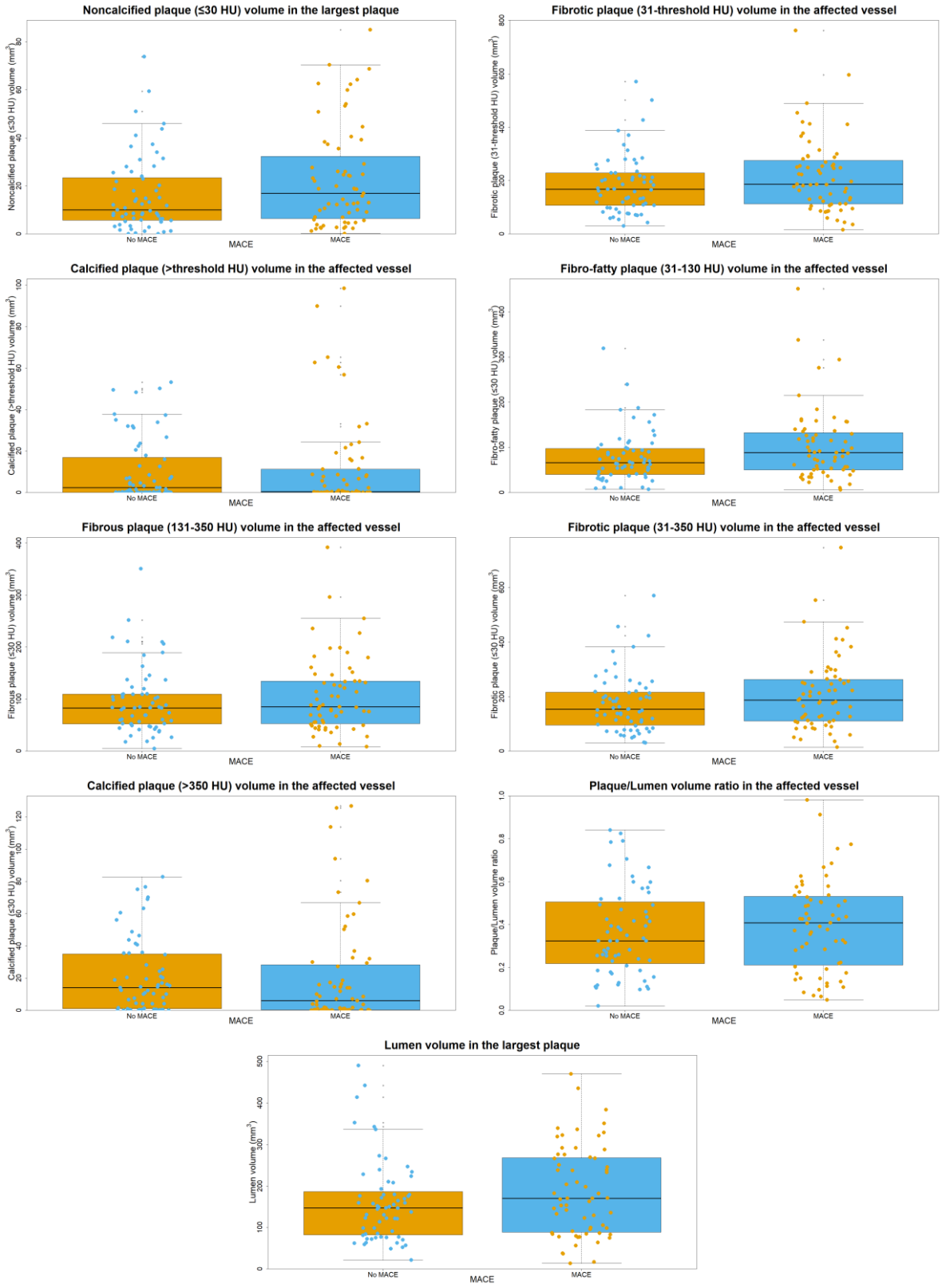

Figure 10: Boxplots illustrating the distribution of different categories of plaque volume, lumen volume, and plaque/lumen ratio across the no MACE on the left and the MACE group on the right of each boxplot. Every boxplot illustrates a different plaque volume category for the coronary artery that had the largest plaque.

None of the plaque categories showed a significant difference between the no MACE and MACE group. However, several trends were observed that warrant further attention. The closest to significance was the noncalcified plaque category (<30 HU), which had a p-value of 0.051 in Mood's median test and 0.070 in the Wilcoxon test. Similarly, the fibro-fatty plaque (31-130 HU) showed trends toward significance with p-values of 0.110 and 0.067, respectively, for the two tests. Calcified plaque (>350 HU) also was almost significant, as the p-values of the Mood's median test and Wilcoxon test were p = 0.076, and p = 0.211 respectively. Other plaque categories had p-values > 0.2 indicating that these categories do not have such a strong association with the occurrence of MACE.

These findings suggest that while the differences in plaque volumes between MACE and no-MACE groups are not statistically significant, certain trends in specific plaque categories, particularly noncalcified (<30 HU) and fibro-fatty plaques (31-130 HU), and calcified plaques (>350 HU) may be clinically relevant and have an association with the outcome MACE. Table 11 presents the median values, interquartile ranges, and p-values from both Mood's median test and the Wilcoxon test for all plaque categories. This table details the median plaque volumes for both groups and their corresponding statistical significance.

Table 11: Comparison of plaque characteristics between MACE and no MACE groups for all patients. The table presents the median values of various plaque volumes for both the non-MACE and MACE groups. Additionally, it includes the p-values from Mood's median test, and the p-values from the Mann-Whitney U test.

Variable (HU thresholds)	**Median no MACE**	**Median MACE**	**p-value Mood's median test**	**p-value Mann-Whitney U test**
Affected vessel Noncalcified plaque (<30 HU)	16.1 (22.4)	24.50 (27.1)	0.051	0.070
Affected vessel Fibrotic plaque (31-threshold HU)	167.4 (121.6)	186.7 (162.9)	0.214	0.151
Affected vessel calcified plaque (>threshold HU)	2.4 (16.9)	0.4 (11.3)	0.214	0.426
Affected vessel Fibro-fatty plaque (31-130 HU)	65.9 (57.4)	88.3 (82.1)	0.110	0.067
Affected vessel fibrous plaque (131-350 HU)	82.8 (57.4)	85.0 (81.6)	0.595	0.438
Affected vessel fibrotic plaque (31-350 HU)	153.7 (120.6)	186.7 (152.7)	0.214	0.135
Affected vessel calcified plaque (>350 HU)	14.1 (33.9)	6.0 (27.9)	0.076	0.211
Affected vessel lumen volume	608.9 (352.2)	675.7 (485.2)	0.214	0.299
Affected vessel plaque/lumen	0.32 (0.29)	0.41 (0.32)	0.214	0.421

Discussion

In this study, we found that three plaque categories, noncalcified plaque (<30 HU), fibro-fatty plaque (31-130 HU), and calcified plaque (>350 HU), may be clinically relevant and associated with the outcome of MACE. Noncalcified and fibro-fatty plaques were generally larger in patients who experienced a MACE after their CCTA, whereas calcified plaques were generally smaller in these patients as demonstrated by our results. Additionally, we discovered that the automatic threshold determined by the GE AW software for distinguishing between fibrotic and calcified plaque is explained by the luminal attenuation in the aorta.

We found that the automatic threshold used in the GE AW server software is predominantly based on the attenuation of the lumen as shown in Figure 9, Table 8, and Table 9. Intravascular attenuation has a high correlation with the attenuation of coronary atherosclerotic plaques as shown by Cademartiri et al. [22]. The variability in intracoronary attenuation can lead to differences in the measured plaque volumes per category when standardized thresholds are used when comparing patients. This variability is caused by the partial volume effect where different materials within one voxel are interpolated, leading to inaccuracies. Therefore, it would be logical to use a threshold that adapts to the intravascular attenuation.

Our results revealed that standardized thresholds result in lower p-values compared to the automatic threshold plaque categories, determined by the GE AW server software, when comparing the no MACE and MACE groups as shown in Table 11. This suggests that standardized thresholds may provide more consistent and statistically significant results. However, the influence of intravascular attenuation on plaque measurements underscores the importance of using standardized imaging protocols to minimize variability and improve the reliability of comparisons between patient groups when using standardized thresholds.

Our results showed that noncalcified plaque (<30 HU) and fibro-fatty plaque (31-130 HU) volumes have an almost statistically significant difference between the no MACE and MACE group in our study. This finding can be explained by the nature of these plaques. As these plaques are softer, they are more prone to wear and tear, which can lead to plaque rupture. Such ruptures can result in the formation of a thrombus, potentially causing a MACE [14].

This is also found by Deseive et al [48]. They combined fibrotic plaque and noncalcified plaque into one category, called noncalcified plaque. They found a significant difference between the group without a MACE and the group with a MACE ($p < 0.001$). They however included all patients who underwent a CCTA in a specific time period. Therefore their group with no cardiac event is much larger than the group with a cardiac event (1518 vs 59 patients). This can introduce bias since there is an imbalance in group sizes.

Furthermore, the larger sample size increases the likelihood of including more patients with smaller plaque volumes in the no MACE group, thereby enhancing the probability of detecting a significant difference between the no MACE and MACE groups.

Motoyama et al. conducted a study examining the relationship between low attenuation plaque volume, also referred to as noncalcified plaque volume, and the incidence of acute coronary syndrome (ACS) [49]. ACS was defined as ischemic discomfort presenting with elevation of troponin level, and ischemic discomfort that was Canadian Cardiology Society class 3 or 4 without elevation of troponin level. Their findings revealed that patients with ACS, as well as those who developed ACS within 0 to 24 months following CCTA, had significantly larger volumes of noncalcified plaque ($p < 0.001$). In contrast to our study, Motoyama et al. included all patients who underwent CCTA, which likely increased the inclusion of more low risk patients. Due to the propensity matching in our study, we have two comparable groups with a similar risk. This methodological difference suggests that Motoyama et al. were more likely to find a significant difference in plaque volumes.

The SCOT-HEART trial further supports the importance of CCTA quantification [50]. The trial demonstrated that low-attenuation plaque burden is the strongest predictor of fatal or nonfatal myocardial infarction. Specifically, the study found that patients with a higher low-attenuation plaque burden were significantly more likely to experience a myocardial infarction compared to those with lower burdens ($p < 0.001$). In contrast to our study, they included patients who had stable chest pain, and did not have a 1:1 matched patient cohort, which makes it more likely to find a difference between the group who experienced myocardial infarction and the group that did not. This does however give a good insight into the role of low-attenuation plaques in predicting cardiovascular events for a larger population. These results highlight the critical role of low-attenuation plaque burden in risk stratification and underscore the need for incorporating this measure into clinical practice to improve the prediction and prevention of adverse cardiovascular events.

A remarkable result in our study is that the calcified plaque volume in general is smaller for the MACE group compared to the no MACE group. However, the MACE group contains some outliers with a larger calcified plaque volume compared to all patients in the no MACE group. This finding is intriguing when compared to the Agatston score, also known as coronary artery calcium score (CACS). In this scoring system, plaques with a CT number of 300-399 HU are assigned 3 points per voxel, while those with a CT number of 400+ HU receive 4 points per voxel, thereby contributing to a higher score and an increased risk of MACE [51]. Kamerman et al. have categorized the different scores into four groups (CACS 0, CACS 1-399, CACS 400-999, and CACS >1000) and found that the MACE rate increased significantly with each higher CACS category [52]. Rosendael et al. also found that calcified plaque volumes were larger in the control group compared to a

ACS group and contributed this finding to the stability of the plaque [17]. Calcified plaques are more stable compared to noncalcified plaques and are therefore associated with a lower risk for ACS.

Limitations

Our study had several limitations. Firstly, the patient group consisted of 126 individuals, from whom we segmented the coronary arteries and measured plaque volumes. We compared a 1:1 matched cohort based on risk factors. Consequently, our results are not applicable to the entire patient population, as our study cohort has a relatively high risk profile. Although we did not find any statistically significant differences overall, some plaque categories showed trends towards significance between the no MACE and MACE group. With a larger patient population, these trends would likely reach statistical significance, thereby providing more definitive insights into the differences in plaque characteristics between the two groups. This limitation underscores the need for further research with larger sample sizes to validate our findings and enhance the generalizability of the results.

Secondly, we had to manually adjust the segmentation of multiple patients. This manual intervention introduces a potential source of variability, which can affect the reproducibility of our study. The need for manual adjustments to the segmentation highlights the challenges in achieving consistent and automated segmentation. Furthermore, we found significant differences between the software we used (AW server) and Medis QAngio CT plaque analysis. When we measured two patients in both software packages, we observed differences in all plaque categories and lumen volumes. This suggests that the software used for plaque quantification can also introduce variability in the plaque volumes measured. Therefore, it is important to avoid comparing plaque volumes measured with different software packages to ensure consistency and accuracy in the results.

Thirdly, in our study, we did not take the tube voltage into account, since it had no significant effect on the measured plaque volumes. However, multiple articles have shown that the tube voltage can have an effect on the measured plaque volumes [53, 54].

Additionally, the study was performed at a single center (Isala hospital). The patient population and clinical practices in Isala may not be representative of other hospitals. Consequently, the results may not be applicable for other hospitals.

Lastly, our study was conducted using images made using the GE Lightspeed VCT XT and Philips Ingenuity CT. Currently, CCTA scans in Isala hospital are mostly made using the GE Revolution Apex CT, which has a wider detector and newer deep learning reconstruction algorithms that may affect the plaque characteristics and volumes [55, 56].

Clinical implications

The findings of our study have several clinical implications. Firstly, we found that the standardized thresholds (noncalcified plaque (<30 HU), fibro-fatty plaque (31-130 HU), and calcified plaque (>350 HU)) resulted in the lowest p-values, and these are potentially clinically relevant and associated with MACE outcomes. Noncalcified and fibro-fatty plaques were generally larger in patients who experienced a MACE after their CCTA scan, whereas calcified plaques were generally smaller in these patients. This suggests that plaque composition and volume could serve as biomarkers for predicting adverse cardiovascular events, aiding in risk stratification and personalized patient management.

Secondly, while we did not find a significant effect of tube voltage on plaque volumes, existing literature suggests otherwise [53, 54]. Clinicians should consider the potential impact of imaging parameters, such as tube voltage, on plaque measurements. Future research should aim to clarify these effects to ensure that plaque quantification is accurate and comparable across different imaging settings.

Lastly, advancements in imaging technology, such as the use of the GE Revolution Apex CT with its wider detector and deep learning reconstruction algorithms, may influence plaque characteristics. Clinicians should stay informed about these technological developments and consider their potential impact on plaque assessment. Future studies should incorporate these newer technologies to provide relevant and up-to-date insights into plaque characteristics and their clinical implications.

Future perspectives

Larger cohort studies should be performed to validate the trends observed in plaque volumes between the no MACE and MACE groups in our study. This could help establish more definitive biomarkers for predicting adverse cardiovascular events.

Secondly, the variability introduced by manual segmentation adjustments and differences between software packages underscores the need for standardized and automated plaque quantification methods. Clinicians should be aware of these potential sources of variability and consider them when interpreting plaque volume measurements. The development and adoption of more consistent and reliable segmentation tools could improve the accuracy and reproducibility of plaque assessments, ultimately enhancing clinical decision-making. New software packages like Cleerly AI-guided quantitative CCTA (AI-QCT), which automatically performs CCTA analysis, can potentially help with this problem [57]. With this software, a lot of time can be saved, and insights into plaque characteristics can be obtained more efficiently.

In this study we performed plaque quantification using conventional CT, which shows CT numbers per voxel. However, using dual-energy CT, material decomposition can be applied to the CCTA scans, allowing for a more detailed and precise analysis of plaques [58]. This technique enables the differentiation of various plaque components, such as calcium, lipid, and fibrous tissue, providing a more comprehensive understanding of plaque composition and potentially improving the assessment of plaque stability and the risk of cardiovascular events. This method is also independent from the lumen attenuation which is a large advantage.

Pericoronary adipose tissue (PCAT) attenuation is a promising new imaging marker [59]. Measured in Hounsfield units (HU), it reflect coronary inflammation, with higher values indicating increased risk of adverse cardiovascular events. Future studies should standardize PCAT measurements protocols and validate its prognostic value in diverse populations. Another promising new imaging marker is CT-derived fractional flow reserve (CT-FFR) [60]. Using deep learning techniques, the coronary arteries are segmented from the CCTA scan, and computational fluid dynamics are applied to calculate the blood flow reduction caused by any blockage in the coronary arteries.

Conclusion

Although we did not find a significant difference in plaque volume between the group that did not experience a MACE after CCTA and the group that did experience a MACE after CCTA, observable trends were present. Non-calcified plaque volumes (< 30 HU) and fibro-fatty plaque volumes (31-130 HU) were generally larger in the MACE group. Additionally, we found that the calcified plaque volumes (>350 HU) were generally smaller in the MACE group compared to the no MACE group.

References

[1] Byrne RA, Rossello X, Coughlan JJ, et al. 2023 ESC Guidelines for the management of acute coronary syndromes: Developed by the task force on the management of acute coronary syndromes of the European Society of Cardiology (ESC). *Eur Heart J* 2023; 44: 3720–3826.

[2] Koop Y, Wimmers RH, Vaartjes I, et al. *Cijferboek hart- en vaatziekten in Nederland 2021*. Den Haag, December 2021.

[3] StatLine - Overledenen; belangrijke doodsoorzaken (korte lijst), leeftijd, geslacht, https://opendata.cbs.nl/statline/#/CBS/nl/dataset/7052_95/table?fromstatweb (accessed 11 December 2024).

[4] Vrints C, Andreotti F, Koskinas KC, et al. 2024 ESC Guidelines for the management of chronic coronary syndromes: Developed by the task force for the management of chronic coronary syndromes of the European Society of Cardiology (ESC) Endorsed by the European Association for Cardio-Thoracic Surgery (EACTS). *Eur Heart J* 2024; 45: 3415–3537.

[5] Virani SS, Newby LK, Arnold S V., et al. 2023 AHA/ACC/ACCP/ASPC/NLA/PCNA Guideline for the Management of Patients With Chronic Coronary Disease: A Report of the American Heart Association/American College of Cardiology Joint Committee on Clinical Practice Guidelines. *Circulation* 2023; 148: E9–E119.

[6] Cury RC, Leipsic J, Abbara S, et al. CAD-RADS™ 2.0 – 2022 Coronary Artery Disease – Reporting and Data System An Expert Consensus Document of the Society of Cardiovascular Computed Tomography (SCCT), the American College of Cardiology (ACC), the American College of Radiology (ACR) and the North America Society of Cardiovascular Imaging (NASCI). *Radiol Cardiothorac Imaging*; 4. Epub ahead of print 1 October 2022. DOI: 10.1148/RYCT.220183.

[7] Szilveszter B, Kolossváry M, Pontone G, et al. How to quantify coronary atherosclerotic plaque using computed tomography. *Eur Heart J Cardiovasc Imaging* 2022; 23: 1573–1575.

[8] Hsieh J. *Computed Tomography, Second Edition*. 1000 20th Street, Bellingham, WA 98227-0010 USA: SPIE, 2009. Epub ahead of print 26 October 2009. DOI: 10.1117/3.817303.

[9] Rhee DJ, Kim S, Moon YM, et al. Effects of the difference in tube voltage of the CT scanner on dose calculation, https://arxiv.org/abs/1503.03563v1 (2015, accessed 29 November 2024).

[10] Abbene L, Kris Iniewski K. High-Z Materials for X-ray Detection: Material Properties and Characterization Techniques. *High-Z Materials for X-ray Detection: Material Properties and Characterization Techniques* 2023; 1–246.

[11] Villines TC, Robinson AA. Will Plaque Quantification on Coronary CTA End Our Infatuation With Lumen Stenosis? *JACC Cardiovasc Imaging* 2020; 13: 1718–1720.

[12] Frink RJ. The Beginnings. A Multicentric Disease, https://www.ncbi.nlm.nih.gov/books/NBK2029/ (2002, accessed 14 December 2023).

[13] van Veelen A, van der Sangen NMR, Henriques JPS, et al. Identification and treatment of the vulnerable coronary plaque. *Rev Cardiovasc Med* 2022; 23: 39.

[14] Coronary Artery Disease - StatPearls - NCBI Bookshelf, https://www.ncbi.nlm.nih.gov/books/NBK564304/ (accessed 14 December 2023).

[15] Liverpool Heart and Chest Hospital | Coronary Artery Disease, https://www.lhch.nhs.uk/coronary-artery-disease (accessed 10 January 2024).

[16] Mohan J, Shams P, Bhatti K, et al. Coronary Artery Calcification. *StatPearls*, https://www.ncbi.nlm.nih.gov/books/NBK519037/ (2024, accessed 3 January 2025).

[17] Van Rosendael AR, Narula J, Lin FY, et al. Association of High-Density Calcified 1K Plaque With Risk of Acute Coronary Syndrome. *JAMA Cardiol* 2020; 5: 282.

[18] Giusca S, Schütz M, Kronbach F, et al. Coronary Computer Tomography Angiography in 2021—Acquisition Protocols, Tips and Tricks and Heading beyond the Possible. *Diagnostics* 2021; 11: 1072.

[19] Dey D, Lee CJ, Ohba M, et al. Image quality and artifacts in coronary CT angiography with dual-source CT: Initial clinical experience. *J Cardiovasc Comput Tomogr* 2008; 2: 105–114.

[20] Hsieh J. *Computed Tomography, Second Edition*. 1000 20th Street, Bellingham, WA 98227-0010 USA: SPIE, 2009. Epub ahead of print 26 October 2009. DOI: 10.1117/3.817303.

[21] Attix FH. Introduction to Radiological Physics and Radiation Dosimetry. *Introduction to Radiological Physics and Radiation Dosimetry*. Epub ahead of print 19 November 1986. DOI: 10.1002/9783527617135.

[22] Cademartiri F, Mollet NR, Runza G, et al. Influence of intracoronary attenuation on coronary plaque measurements using multislice computed tomography: Observations in an ex vivo model of coronary computed tomography angiography. *Eur Radiol* 2005; 15: 1426–1431.

[23] Cademartiri F, Mollet NR, Runza G, et al. Influence of intracoronary attenuation on coronary plaque measurements using multislice computed tomography: Observations in an ex vivo model of coronary computed tomography angiography. *Eur Radiol* 2005; 15: 1426–1431.

[24] Computed Tomography (CT), https://www.nibib.nih.gov/science-education/science-topics/computed-tomography-ct (accessed 3 December 2024).

[25] What are the benefits of CT scans?, https://www.radiologyinfo.org/en/info/safety-hiw_04 (accessed 3 December 2024).

[26] Murakami Y, Kakeda S, Kamada K, et al. Effect of Tube Voltage on Image Quality in 64-Section Multidetector 3D CT Angiography: Evaluation with a Vascular Phantom with Superimposed Bone Skull Structures. *American Journal of Neuroradiology* 2010; 31: 620–625.

[27] Lira D, Padole A, Kalra MK, et al. Tube Potential and CT Radiation Dose Optimization. *American Journal of Roentgenology* 2015; 204: W4–W10.

[28] Kaza RK, Platt JF, Goodsitt MM, et al. Emerging techniques for dose optimization in abdominal CT. *Radiographics* 2014; 34: 4–17.

[29] Calicchio F, Hu E, Newlander S, et al. The effect of tube voltage on scan–rescan reproducibility of compositional plaque volume: technical variability is not true biological change. *European Heart Journal - Imaging Methods and Practice*; 2. Epub ahead of print 16 January 2024. DOI: 10.1093/EHJIMP/QYAE041.

[30] Gao Y, Pan Y, Jia C. Influencing factors and improvement methods of coronary artery plaque evaluation in CT. *Front Cardiovasc Med* 2024; 11: 1395350.

[31] Pan Y, Gao Y, Wang Z, et al. Effects of low-tube voltage coronary CT angiography on plaque and pericoronary fat assessment: intraindividual comparison. *Eur Radiol* 2024; 34: 5713–5723.

[32] Boas FE, Fleischmann D. CT artifacts: causes and reduction techniques. *Imaging Med* 2012; 4: 229–240.

[33] Afifi MB, Abdelrazek A, Deiab NA, et al. The effects of CT x-ray tube voltage and current variations on the relative electron density (RED) and CT number conversion curves. *J Radiat Res Appl Sci* 2020; 13: 1–11.

[34] NIST: X-Ray Mass Attenuation Coefficients - Table 4, https://physics.nist.gov/PhysRefData/XrayMassCoef/tab4.html (accessed 27 November 2024).

[35] Sellerer T, Noël PB, Patino M, et al. Dual-energy CT: a phantom comparison of different platforms for abdominal imaging. *Eur Radiol* 2018; 28: 2745–2755.

[36] Roa AMA, Andersen HK, Martinsen ACT. CT image quality over time: comparison of image quality for six different CT scanners over a six-year period. *J Appl Clin Med Phys* 2015; 16: 350–365.

[37] Mangla A, Oliveros E, Williams KA, et al. Cardiac Imaging in the Diagnosis of Coronary Artery Disease. *Curr Probl Cardiol* 2017; 42: 316–366.

[38] Marano R, Rovere G, Savino G, et al. CCTA in the diagnosis of coronary artery disease. *Radiologia Medica* 2020; 125: 1102–1113.

[39] Nurmohamed NS, van Rosendael AR, Danad I, et al. Atherosclerosis evaluation and cardiovascular risk estimation using coronary computed tomography angiography. *Eur Heart J* 2024; 45: 1783–1800.

[40] Moon SJ, Chun EJ, Yoon YE, et al. Long-Term Prognostic Value of Coronary Computed Tomography Angiography in an Asymptomatic Elderly Population. *Journal of the American Heart Association: Cardiovascular and Cerebrovascular Disease* 2019; 8: e013523.

[41] Antonopoulos AS, Simantiris S. Preventative Imaging with Coronary Computed Tomography Angiography. *Curr Cardiol Rep* 2023; 25: 1623–1632.

[42] Abdelrahman KM, Chen MY, Dey AK, et al. Coronary Computed Tomography Angiography From Clinical Uses to Emerging Technologies: JACC State-of-the-Art Review. *J Am Coll Cardiol* 2020; 76: 1226–1243.

[43] Nurmohamed NS, van Rosendael AR, Danad I, et al. Atherosclerosis evaluation and cardiovascular risk estimation using coronary computed tomography angiography. *Eur Heart J* 2024; 45: 1783–1800.

[44] Austin PC. Optimal caliper widths for propensity-score matching when estimating differences in means and differences in proportions in observational studies. *Pharm Stat* 2011; 10: 150–161.

[45] GE Healthcare. *AW server 3.2 User Manual revision 12*. 2022.

[46] Mood AM. On the Asymptotic Efficiency of Certain Nonparametric Two-Sample Tests. *The Annals of Mathematical Statistics* 1954; 25: 514–522.

[47] Wilcoxon F. Individual Comparisons by Ranking Methods. *Biometrics Bulletin* 1945; 1: 80.

[48] Deseive S, Kupke M, Straub R, et al. Quantified coronary total plaque volume from computed tomography angiography provides superior 10-year risk stratification. *Eur Heart J Cardiovasc Imaging* 2021; 22: 314–321.

[49] Motoyama S, Sarai M, Harigaya H, et al. Computed Tomographic Angiography Characteristics of Atherosclerotic Plaques Subsequently Resulting in Acute Coronary Syndrome. *J Am Coll Cardiol* 2009; 54: 49–57.

[50] Williams MC, Kwiecinski J, Doris M, et al. Low-Attenuation Noncalcified Plaque on Coronary Computed Tomography Angiography Predicts Myocardial Infarction: Results From the Multicenter SCOT-HEART Trial (Scottish Computed Tomography of the HEART). *Circulation* 2020; 141: 1452.

[51] Agatston AS, Janowitz WR, Hildner FJ, et al. Quantification of coronary artery calcium using ultrafast computed tomography. *J Am Coll Cardiol* 1990; 15: 827–832.

[52] Kamerman M, van Dijk JD, Timmer JR, et al. The incremental value of coronary artery calcium score in predicting long-term prognosis and defining the warranty period of normal adenosine stress-only myocardial perfusion imaging using CZT SPECT. *Journal of Nuclear Cardiology* 2023; 30: 2692–2701.

[53] Tanami Y, Ikeda E, Jinzaki M, et al. Computed tomographic attenuation value of coronary atherosclerotic plaques with different tube voltage: An ex vivo study. *J Comput Assist Tomogr* 2010; 34: 58–63.

[54] Dalager MG, Bøttcher M, Dalager S, et al. Imaging atherosclerotic plaques by cardiac computed tomography in vitro: Impact of contrast type and acquisition protocol. *Invest Radiol* 2011; 46: 790–795.

[55] Cademartiri F, La Grutta LL, Runza G, et al. Influence of convolution filtering on coronary plaque attenuation values: Observations in an ex vivo model of multislice computed tomography coronary angiography. *Eur Radiol* 2007; 17: 1842–1849.

[56] Achenbach S, Boehmer K, Pflederer T, et al. Influence of slice thickness and reconstruction kernel on the computed tomographic attenuation of coronary atherosclerotic plaque. *J Cardiovasc Comput Tomogr* 2010; 4: 110–115.

[57] Nurmohamed NS, Danad I, Jukema RA, et al. Development and Validation of a Quantitative Coronary CT Angiography Model for Diagnosis of Vessel-Specific Coronary Ischemia. *JACC Cardiovasc Imaging* 2024; 17: 894–906.

[58] Ding H, Wang C, Malkasian S, et al. Characterization of arterial plaque composition with dual energy computed tomography: a simulation study. *International Journal of Cardiovascular Imaging* 2021; 37: 331–341.

[59] Ma R, Fari R, Van Der Harst P, et al. Evaluation of pericoronary adipose tissue attenuation on CT. *British Journal of Radiology*; 96. Epub ahead of print 1 May 2023. DOI: 10.1259/BJR.20220885/7469099.

[60] Driessen RS, Danad I, Stuijfzand WJ, et al. Comparison of Coronary Computed Tomography Angiography, Fractional Flow Reserve, and Perfusion Imaging for Ischemia Diagnosis. *J Am Coll Cardiol* 2019; 73: 161–173.